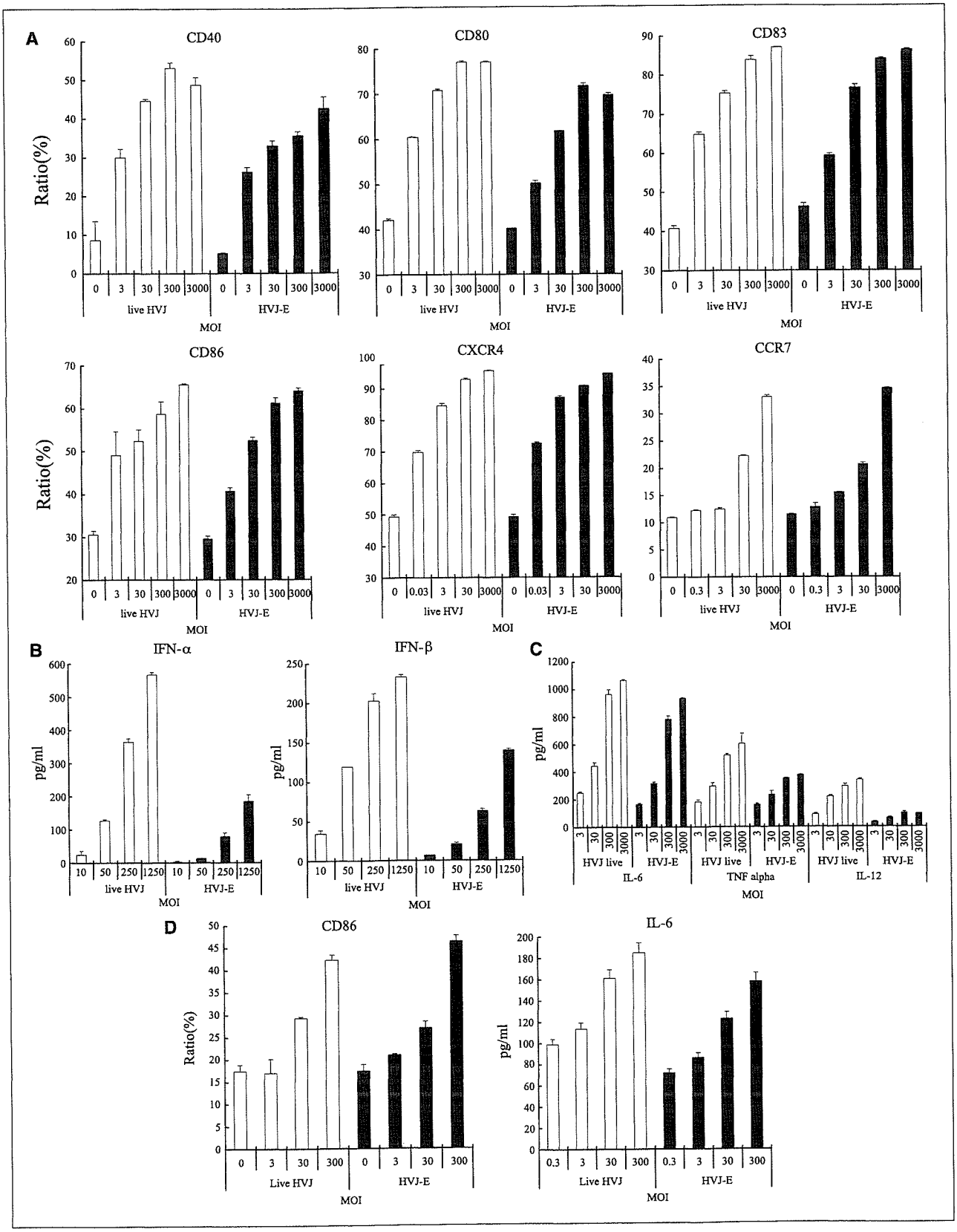
A
CD40
CD80
CD83
CD86
CXCR4
CCR7
Ratio(%)
live HVJ
HVJ-E
MOI
B
IFN-α
IFN-β
pg/ml
C
IL-6
TNF alpha
IL-12
HVJ live
D
CD86
IL-6
Live HVJ

HVJ-E maintained the ability of live HVJ to induce maturation and IL-6 release from murine and human dendritic cells. We examined how HVJ-E induced host antitumor immunity. The recognition of pathogens by antigen presenting cells (APC) is a pivotal initial step in activating innate immunity and for inducing specific acquired immunity (21, 22). We therefore examined the maturation and cytokine release from murine myeloid dendritic cells induced by HVJ-E and then compared the findings with those of live HVJ. We incubated HVJ-E or live HVJ with dendritic cells in culture medium for 48 h and then stained them to analyze CD40, CD80, CD83, CD86, CXCR4, and CCR7 molecules on the dendritic cell surface by FACS. All markers of dendritic cell maturation were dose-dependently increased by HVJ-E and live HVJ (Fig. 2*A*). These results suggest that HVJ-E retains the ability of live HVJ to induce dendritic cell maturation. We measured the amounts of type I IFNs (IFN-α and IFN-β) and representative proinflammatory cytokines (IL-6, TNF-α, or IL-12) released into dendritic cell culture medium at 24 h after adding HVJ-E or live HVJ. The secretion of all of these cytokines was decreased by HVJ-E. However, the decrease in the amount of released IL-6 was minimal and comparable to that released in the presence of live HVJ (Fig. 2*B* and *C*). Next, we measured CD86 expression and IL-6 secretion in human dendritic cells at 48 h after adding HVJ-E or live HVJ-E to the culture medium. CD86 was dose-dependently increased by HVJ-E as well as by live HVJ. The secretion of IL-6 was enhanced by both live HVJ and HVJ-E as seen in murine dendritic cells (Fig. 2*C*) although the total amount of IL-6 in human dendritic cells was lower than that in murine dendritic cells (Fig. 2*D*).

HVJ-E promoted dendritic cell and T-cell recruitment to tumor beds and induced tumor-specific CTLs *in vivo*. To determine how the host adaptive immune system reacts to HVJ-E *in vivo*, the mRNA expression of CD11c as markers for dendritic cells and of CD4 and CD8 for effector T cells was measured in CT26 tumors in mice at 24, 48, and 120 h after HVJ-E injection. CD11c and CD4 expression was significantly increased in tumors treated with HVJ-E compared with saline at all time points with a peak at 48 h. CD8 expression was also significantly increased in the group given HVJ-E. Moreover, the expression level remained maximal even at 120 h after treatment (Fig. 3*A*). Immunohistochemical staining was done to evaluate dendritic cell and T-cell infiltration into tumor tissue after HVJ-E treatment. It revealed that $CD11b^+$, $CD11c^+$, $CD4^+$, or $CD8^+$ cells were remarkably infiltrated into tumor by HVJ-E treatment (Fig. 3*B*). We then did CTL assays and measured standard ^{51}Cr release to determine whether CT26-specific cellular immunoreactions were induced. A CT26-specific CTL response was elicited only in those mice in which CT26 tumors were eradicated by HVJ-E (Fig. 3*C*). Next, we examined the contribution of $CD8^+$ T cells and $CD4^+$ T cells to HVJ-E-induced antitumor effects. SCID mice were reconstituted with $CD8^+$ T cells with or without $CD4^+CD25^-$ T cells obtained from naïve BALB/c mice. After CT26 inoculation and HVJ-E treatment, $CD8^+$ T cells were isolated from spleen and the number of IFN-γ-secreting $CD8^+$ T cells was counted by ELISPOT assay. As a result, significant increase of CT26-specific IFN-γ-secretion from $CD8^+$ T cells was observed only when $CD8^+$ T cells were transferred with $CD4^+CD25^-$ T cells. It revealed that HVJ-E enhanced tumor-specific $CD8^+$ T-cell response in a $CD4^+CD25^-$ T cell–dependent manner (Fig. 3*D*). All of these findings indicated that HVJ-E induced dendritic cell and $CD4^+$ and $CD8^+$ T-cell migration to the tumor site and also activated tumor-specific adaptive T cell–mediated immune responses *in vivo*. It was evident that tumor-specific $CD8^+$ T-cell activation was elicited by HVJ-E in a $CD4^+CD25^-$ T cell–dependent manner.

HVJ-E rescued effector T-cell proliferation from Treg-mediated immunosuppression *in vitro* and *in vivo* through the ability to release IL-6 from dendritic cells. Induction of APC maturation is not the only mechanism that controls T-cell activation because Treg also controls T-cell responses (23–26). IL-6 release from dendritic cells is critical for overcoming the $CD4^+CD25^+$ Treg–mediated immunosuppression of effector T cells (27). Because HVJ-E retained the ability of live HVJ to promote IL-6 release from dendritic cells, we examined whether HVJ-E could inhibit Treg-mediated immunosuppression. T-cell proliferation was assayed using various ratios of Tregs ($CD4^+CD25^+$) to responder T cells ($CD4^+CD25^-$) in the presence of splenic $CD11c^+$ cells as APCs and anti-CD3 antibodies. Before evaluating T-cell proliferation, we stained the isolated $CD4^+CD25^+$ T cells with anti-Foxp3 antibody because Foxp3 is nowadays considered to be the most specific marker for Treg (25). As a result, the majority of sorted $CD4^+CD25^+$ T cells was confirmed to be $Foxp3^+CD4^+CD25^+$ Tregs (Fig. 4*A*). T-cell proliferation determined by incorporation of $[^3H]$thymidine was gradually suppressed as the ratio of Tregs to responder T cells increased. We confirmed that adding mouse recombinant IL-6 to the T-cell culture medium reversed the Treg-mediated suppression and restored T-cell proliferation to near normal levels. This ability of IL-6 was abrogated by IL-6 neutralizing antibodies (Fig. 4*B*; ref. 27). Next, we examined the reversal of Treg-mediated suppression using conditioned medium from dendritic cells stimulated with HVJ-E (H-DCCM). We found that H-DCCM also reversed Treg-mediated suppression and that IL-6 neutralizing antibodies blocked this restorative effect (Fig. 4*C*). These results indicated that soluble factors in H-DCCM could block Treg-mediated immunosuppression and that IL-6 was dominant for this blockade. We examined IL-6 secretion from dendritic cells after HVJ-E administration *in vivo*. HVJ-E was injected into CT26 tumors in the mouse hind footpad for 3 successive days. Dendritic cells were purified from tumor tissues or drainage lymph nodes at 24 h after the last injection. Intracellular IL-6 was positive in the sorted $CD11c^+$ cells, which were analyzed by FACS. The ratio (%) of IL-6-positive dendritic cells was significantly increased in tumors and drainage lymph nodes by HVJ-E compared with saline (Fig. 5*A*). Next, we examined whether HVJ-E indeed contributed to blocking Treg-mediated immunosuppression *in vivo*. $CD4^+CD25^+$ Tregs and $CD4^+CD25^-$ effector cells were purified from tumor drainage lymph

Figure 2. Activation of murine and human dendritic cells by HVJ-E. *A*, CD40, CD80, CD83, CD86, CXCR4, or CCR7 expression was measured by FACS analysis after 48 h of coculture with HVJ-E or live HVJ. Bone marrow–derived murine dendritic cells were dose-dependently maturated by virus particles to express CD40, CD80, CD83, CD86, CXCR4, or CCR7 showing that HVJ-E retained the immunogenicity of live HVJ. *B* and *C*, representative cytokine secretion measured in dendritic cell supernatants by capture ELISA 24 h after coculture with HVJ-E or live HVJ. Amounts of type I IFNs (IFN-α and IFN-β; *B*) and proinflammatory cytokines (IL-6, TNF-α, and IL-12; *C*) were diminished after HVJ-E stimulation compared with live HVJ. The decrease in IL-6 secretion was minimal and comparable with that of live HVJ. *D*, stimulation with HVJ-E caused human dendritic cells derived from PBMC to maturate, dose-dependently express CD86, and release IL-6 within 24 h. Human dendritic cells were dose-dependently maturated by virus particles to express CD86 showing that HVJ-E retained the ability of live HVJ. The decrease in IL-6 secretion was minimal and comparable with that of live HVJ. *Columns*, mean of triplicate samples; *bars*, SE. Representative of three independent experiments.

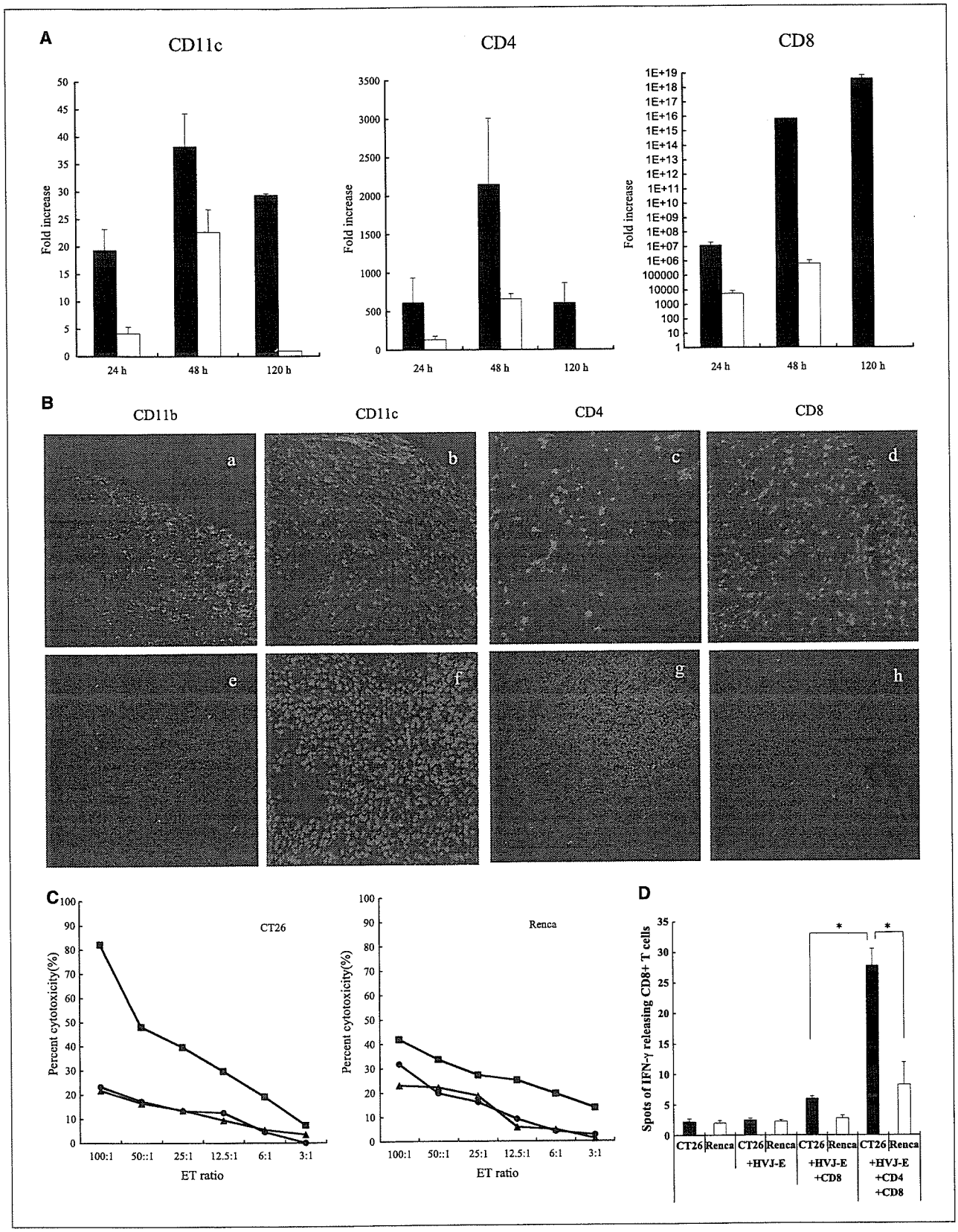
A
CD11c
CD4
CD8
Fold increase
24 h
48 h
120 h
B
CD11b
CD11c
CD4
CD8
a
b
c
d
e
f
g
h
C
CT26
Renca
Percent cytotoxicity(%)
ET ratio
100:1
50::1
25:1
12.5:1
6:1
3:1
D
Spots of IFN-γ releasing CD8+ T cells
CT26
Renca
CT26 +HVJ-E
Renca
CT26 +HVJ-E +CD8
Renca
CT26 +HVJ-E +CD4 +CD8
Renca

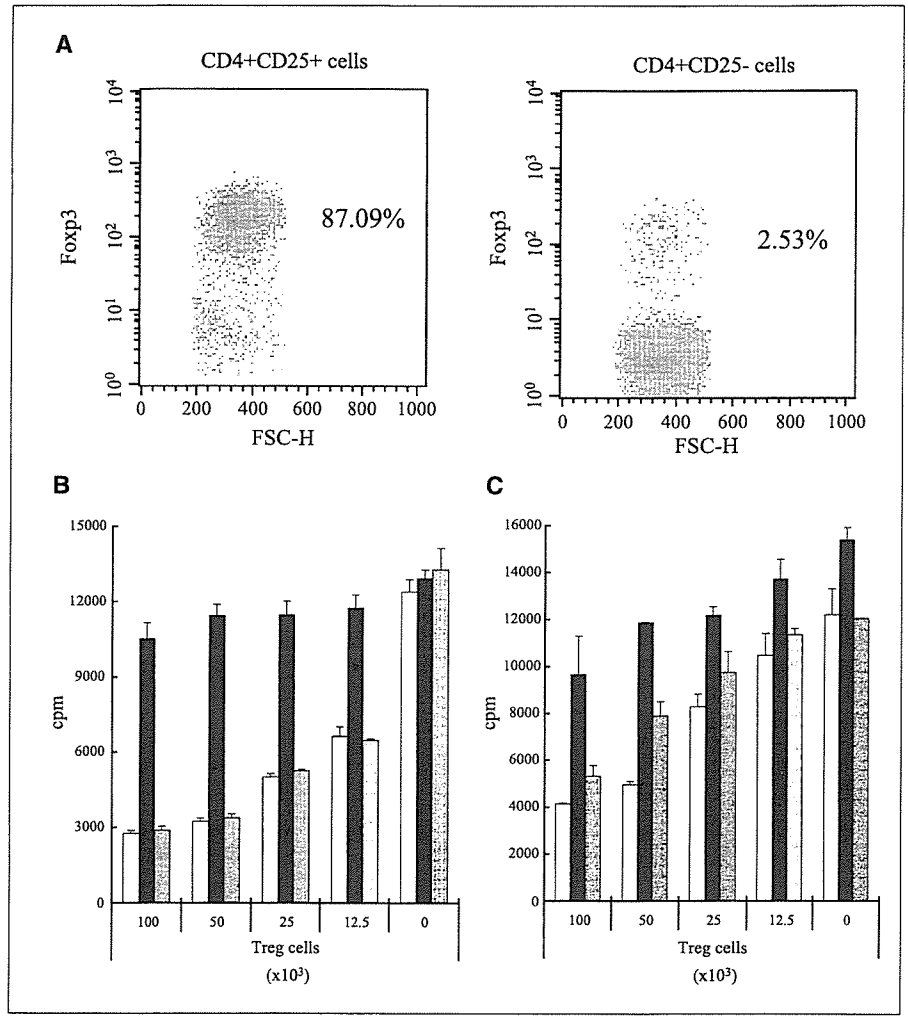

Figure 4. Suppression of regulatory T cells by HVJ-E *in vitro*. *A*, intracellular staining of Foxp3 for purified $CD4^+CD25^+$ cells or $CD4^+CD25^-$ cells. FACS analysis revealed that the majority of $CD4^+CD25^+$ cells isolated by magnetic microbeads was $Foxp3^+CD4^+CD25^+$ Tregs. *B*, $CD4^+CD25^-$ effector T-cell proliferation was suppressed by $CD4^+CD25^+$ Tregs [*open columns*, recombinant IL-6(−)]. Recombinant IL-6 rescued effector T-cell proliferation from the suppression by Tregs [*solid columns*, recombinant IL-6(+)]. This effect was blocked by IL-6 neutralizing antibody (*gray columns*, recombinant IL-6 + anti-IL-6 antibody). *C*, conditioned medium from HVJ-E-stimulated dendritic cells (H-DCCM) rescued $CD4^+CD25^-$ effector T-cell proliferation from $CD4^+CD25^+$ Treg–mediated suppression. This effect was blocked by IL-6 neutralizing antibody. *Open columns*, H-DCCM(−); *solid columns*, H-DCCM(+); *gray columns*, H-DCCM + anti-IL-6 antibody. *Columns*, mean T-cell proliferative responses of triplicate samples; *bars*, SE.

nodes by magnetic cell sorting at 24 h after HVJ-E injections as described above. The suppressive effect of Treg against effector T cells was significantly reduced in HVJ-E-treated mice compared with saline-treated or naïve mice (Fig. 5*B*). Finally, we examined whether an *in vivo* IL-6 neutralization reduces antitumor effect of HVJ-E. Because blockade of IL-6 signaling with IL-6R antibody was reported to recover Treg-mediated immunosuppression *in vivo* (28), 20 μg of IL-6R antibody were injected into tumors simultaneously with HVJ-E on days 4, 8, and 12. We found that blockade of IL-6 signaling significantly reduced HVJ-E-mediated tumor growth inhibition *in vivo* (Fig. 5*C*). These results revealed that HVJ-E was responsible for rescuing effector T-cell proliferation from Treg-mediated immunosuppression. The mechanism through which Treg was suppressed was presumably due to HVJ-E-induced IL-6 secretion from dendritic cells in tumors and drainage lymph nodes.

Discussion

HVJ-E is derived from UV-inactivated HVJ particles. Irradiation with UV breaks the genome of HVJ and removes its ability to

Figure 3. Dendritic cell and T-cell infiltration into tumor beds and induction of tumor-specific CTLs *in vivo*. *A*, mRNA expression quantified by real-time PCR in tumors growing in mouse footpads at 24, 48, and 120 h after intratumor injections of 1.5×10^{10} HVJ-E particles or saline for 3 successive days. CD11c expression was significantly higher in HVJ-E-treated tumors at all time points. Expression levels in HVJ-E-treated tumors peaked at 48 h and remained elevated 120 h later. CD4 expression was also significantly higher in HVJ-E-treated tumors at any time point with the peak level at 48 h. CD8 expression obviously increased in HVJ-E-treated tumors and remained elevated for 120 h. Expression levels were normalized by GAPDH. Each value was calculated as fold increase relative to value of saline-treated tumors at 120 h. *Columns*, mean of triplicate samples; *bars*, SE. *Closed columns*, HVJ-E; *open columns*, saline. *B*, histologic findings of tumors. Representative sections of tumors from HVJ-E-treated mice (*a–d*) or saline controls (*e–h*). $CD11b^+$ (*a* and *e*), $CD11c^+$ (*b* and *f*), $CD4^+$ (*c* and *g*), or $CD8^+$ (*d* and *h*) cells were remarkably infiltrated into tumor tissue by HVJ-E treatment. Tumor tissue was isolated at 48 h after HVJ-E or saline injection for 3 successive days. Acetone-fixed frozen section was stained by respective antibodies and Alexa Fluor 488–labeled secondary antibodies. Nuclei were stained by DAPI (magnification, ×200). *C*, CTL activity against CT26 or Renca measured by standard ^{51}Cr release assay. CT26-specific cytotoxicity increased in mice treated with HVJ-E in which tumors were abrogated. Representative of three independent experiments. ■, HVJ-E; ●, saline; ▲, naïve mice. *D*, CT26-specific IFN-γ secretion from $CD8^+$ T cells estimated by ELISPOT assay. SCID mice were reconstituted with $CD8^+$ T cells with or without $CD4^+CD25^-$ T cells. CT26-specific IFN-γ secretion from $CD8^+$ T cells was enhanced by HVJ-E treatment in a $CD4^+CD25^-$ T cell–dependent manner. *, $P < 0.01$.

replicate, thus ensuring effective gene transfer and safety. HVJ-E conserves the complete structure of the live HVJ envelope containing F, HN, and M proteins (9). Here, we tested the feasibility of using the HVJ-E virus envelope feature to induce antitumor immunity.

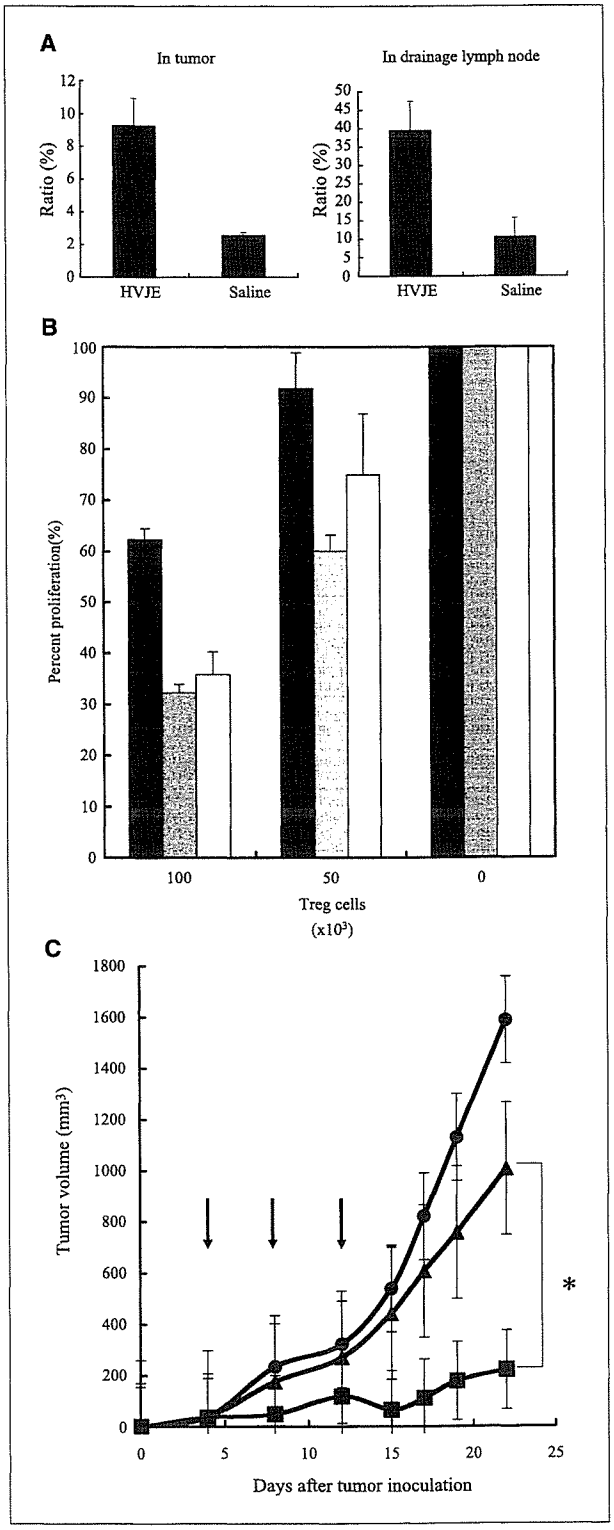

CT26 tumors were eradicated after direct intratumoral injection of HVJ-E. Thus, this strategy alone was sufficient to eliminate established tumors. This property might be unique to Sendai virus particles because the same amount of replication-defective adenovirus had no effect, although the conditions for comparison were limited. We showed that this effect of HVJ-E was due to induced antitumor immune responses because it was abrogated in immunocompromised circumstances such as in SCID mice. None of direct tumor cell killings by activated dendritic cells, macrophages, NK cells, and HVJ-E cell fusion seemed to be predominant because they should be functional in SCID mice (20). Furthermore, the diminished tumorigenesis of CT26 cells co-inoculated distantly from HVJ-E-injected CT26 tumors indicated that the effect of HVJ-E was indirect and that antitumor immunity was enhanced. We also confirmed that cultured CT26 cells were refractory to direct contact with HVJ-E or type I IFNs *in vitro* (13).

The recognition of pathogen-associated molecular patterns by APC such as dendritic cells through Toll-like receptors or retinoic acid-inducible gene I is important to induce not only the activation of innate immunity but also the development of antigen-specific acquired immunity (21, 22). Because we postulated that the activation of APC by HVJ-E or HVJ-E fused cancer cell would be a critical initial step in inducing powerful tumor-specific adaptive immune responses, we examined whether HVJ-E activates dendritic cells and induces tumor-specific immunity. We found that dendritic cells were maturated by HVJ-E to a level comparable to that induced by live HVJ *in vitro*. Furthermore, dendritic cell and effector T-cell recruitment was suggested from the significant increase of CD11c, CD4, and CD8 mRNA expression in mouse tumors injected with HVJ-E. Remarkable infiltrations of dendritic cells and $CD4^+$ and $CD8^+$ T cells into HVJ-E-treated tumors were also confirmed in immunohistochemical studies. Moreover, the significant induction of cancer-specific CTL was observed and $CD8^+$ T cells that depend on $CD4^+CD25^-$ T cells were presumably responsible for this antitumor effect by HVJ-E.

On the other hand, induction of APC maturation is not the only mechanism that controls T-cell activation. T-cell responses are also negatively regulated by Treg (23–26). The accumulation of Treg in tumors or drainage lymph nodes is evidence of their involvement in immune tolerance in patients bearing tumors (29–33), and Treg depletion contributes to enhanced antitumor immunity (34, 35).

Figure 5. Suppression of regulatory T cells by HVJ-E *in vivo*. *A*, ratio (%) of IL-6-secreting $CD11c^+$ cells was significantly increased in tumors and in drainage lymph nodes of mice administered with HVJ-E. $CD11c^+$ cells separated using Macs beads were intracellularly stained with IL-6 and analyzed by FACS at 24 h after HVJ-E was injected into CT26 tumors in mouse footpads for 3 successive days. *Columns*, mean of triplicate samples; *bars*, SE. *B*, $CD4^+CD25^+$ Treg–mediated immunosuppression was reduced in HVJ-E-treated mice *in vivo*. $CD4^+CD25^+$ Tregs and $CD4^+CD25^-$ effector T cells were separated from drainage lymph nodes using Macs beads and then 1×10^5 $CD4^+CD25^-$ T cells were cultured with splenic dendritic cells, anti-CD3 monoclonal antibody, and indicated numbers of $CD4^+CD25^+$ T cells for 48 h. Inhibitory effect of Tregs was significantly reduced in HVJ-E-treated mice *in vivo*. T-cell proliferative responses are expressed as percent of total counts where 100% represents counts in absence of Tregs. *Columns*, mean of triplicate samples; *bars*, SE. Mice treated with (*solid columns*, HVJ-E; *gray columns*, saline; *open columns*, naïve mice). Representative of three independent experiments. *C*, an *in vivo* blockade of IL-6 signaling reduced antitumor effect of HVJ-E. For blocking IL-6 signaling *in vivo*, 20 μg of IL-6R antibody were injected into tumors simultaneously with HVJ-E on days 4, 8, and 12. Tumor volume was measured as previously described. CT26 tumor growth inhibition by HVJ-E was significantly reduced by local injection of IL-6R antibody. *, $P < 0.05$. ■, HVJ-E + control IgG; ▲, HVJ-E + IL-6R antibody; ●, saline. *Arrows*, timing of HVJ-E and IL-6R antibody or control IgG injections. *Points*, mean; *bars*, SE. Results were statistically analyzed using Student's *t* test.

Furthermore, tumor cell–licensed immature dendritic cells are critical for the proliferation and accumulation of Treg in the induction of host immune tolerance against cancer (36). Therefore, overcoming Treg-mediated suppression of antitumor immunoreactions is prerequisite for future cancer immunotherapy. The present study found that H-DCCM rescued effector T-cell proliferation from Treg-mediated immunosuppression and that such rescue was abrogated by IL-6 neutralizing antibody. These results indicated that IL-6 secretion from HVJ-E-treated dendritic cells is key to this inhibitory phenomenon against Treg-mediated suppression. IL-6 is a multifunctional cytokine that regulates immune response, hematopoiesis, acute phase response, and inflammation (37–39), and when released from dendritic cells, IL-6 is critical for overcoming $CD4^+CD25^+$ Treg–mediated immunosuppression (27, 40). In addition, blockade of IL-6 signaling contributes to Treg expansion (28). Here, we found that when dendritic cells were cocultured with HVJ-E, IL-6 secretion levels were comparable to those in the presence of live HVJ, whereas levels of many other cytokines were diminished. We also confirmed that the increase in IL-6 secreted by dendritic cells in tumors and drainage lymph nodes was significant in mice administered with HVJ-E, which also reduced $CD4^+CD25^+$ Treg–mediated inhibition against $CD4^+CD25^-$ effector T-cell proliferation *in vivo*. Moreover, the reduction of HVJ-E-mediated tumor growth inhibition was confirmed by blocking IL-6 signaling with IL-6R antibody *in vivo*. To evaluate the potential side effects by enhanced IL-6 secretion after HVJ-E treatment, the amounts of aspartate aminotransferase, alanine aminotransferase, alkaline phosphatase, total bilirubin, urea nitrogen, and creatinine in serum were measured 1 week after the last HVJ-E injection. There was no significant increase in all these markers of hepatic or renal toxicity in HVJ-E-treated mice. Furthermore, histologic analysis for H&E-stained sections of liver, intestine, and skin showed that no remarkable inflammation or tissue damage was induced by HVJ-E treatment (data not shown).

Lopez et al. reported that CD80 or CD86 costimulatory molecules are normally up-regulated on dendritic cells treated with UV-inactivated Sendai Cantell virus in a manner similar to that of live virus, but unlike UV-inactivated influenza, which is another negative-strand RNA virus. However, the secretion of cytokines including IFN-α, IL-1β, IL-6, IL-12, and TNF-α in dendritic cells was considerably diminished by UV inactivation and they suggested that dendritic cell maturation markers and cytokine release are separately regulated (41). Here, we confirmed that HVJ-E induced normal dendritic cell maturation that was comparable to that induced by live HVJ (Sendai virus). Notably, the level of IL-6 secretion was similar, whereas that of other representative cytokines such as IFN-α, IFN-β, and IL-12 was reduced. Because UV inactivation abrogated the infectivity of HVJ-E as described (9), the notion that live HVJ escaped UV-inactivation and contributed to IL-6 production is unlikely. This discrepancy between our results and theirs might be explained by the choice of HVJ strains (Cantell versus Z strain) or the multiplicity of infection (MOI, 0.6–10 versus 3–3,000). Signal transduction in dendritic cells induced by live HVJ stimulation is independent of Toll-like receptor-3, -7, -8, -9 signaling or of the adaptor protein MyD88 (42). Thus, dendritic cells must use another pathway against HVJ-E stimulation that does not require viral replication. Further investigation should address the detailed molecular mechanisms by which HVJ-E induces dendritic cell maturation and retains IL-6 secretion, and explain the immunologic characteristics of HVJ-E that render it advantageous for cancer treatment. Tumor cell–licensed dendritic cells induce Treg activation through transforming growth factor-β secretion, which helps cancer to escape immune surveillance (35). HVJ-E might reverse this mechanism by inducing IL-6 secretion from dendritic cells in the tumor bed or drainage lymph nodes.

As a delivery vector, HVJ-E can incorporate and directly deliver anticancer drugs to cells through its membrane fusion activity. The cytotoxicity of bleomycin to cancer cells is increased >300-fold in the presence, compared with the absence of HVJ-E (13). HVJ-E also delivers small interfering RNA (siRNA) to cells at high efficiency both *in vitro* and *in vivo*. Delivering Rad51 siRNA using HVJ-E to cancer cells significantly increases their sensitivity to cisplatin (10). Three injections of HVJ-E-containing Rad51 siRNA to tumor masses in SCID mice significantly inhibited tumor growth in the presence of cisplatin and the present study showed that HVJ-E itself enhanced antitumor immunity via multiple pathways.

All of these findings together indicate that HVJ-E alone could induce vigorous antitumor immune responses, an activity that is simultaneously reinforced by inhibiting Treg-mediated immunosuppression. The IL-6 produced by HVJ-E-stimulated dendritic cells was presumably responsible for this reinforcement. Furthermore, the amount of induced immunity was sufficient to eradicate established tumors. Others have described dendritic cell maturation or cytokine release by Sendai virus (41–43), but we are the first to show the potentially remarkable contribution of HVJ-E to cancer treatment through its ability to enhance host immunity. Moreover, the finding that human dendritic cells maturated and released IL-6 after HVJ-E stimulation *in vitro* indicated that clinical applications are possible. Clinical grade HVJ-E is being produced by our venture company (44). The efficient delivery of anticancer reagents and enhanced antitumor immunity indicate that HVJ-E shows promise as a novel cancer therapeutic.

Acknowledgments

Received 5/5/2006; revised 9/1/2006; accepted 11/2/2006.

Grant support: Northern Osaka (Saito) Biomedical Knowledge-Based Cluster Creation Project, Special Coordination Funds for Promoting Science, and the Ministry of Health, Labor, and Welfare of Japan.

The costs of publication of this article were defrayed in part by the payment of page charges. This article must therefore be hereby marked *advertisement* in accordance with 18 U.S.C. Section 1734 solely to indicate this fact.

We thank Dr. Kazunori Aoki for providing the adenovirus and the members of our laboratories for helpful advice and comments.

References

1. Steinman RM, Mellman I. Immunotherapy: bewitched, bothered, and bewildered no more. Science 2004;305:197–200.
2. Blattaman JN, Greenberg PD. Cancer immunotherapy: a treatment for the masses. Science 2004;305:200–5.
3. Pawelec G. Immunotherapy and immunoselection-tumor escape as the final hurdle. FEBS Lett 2004;567:63–6.
4. Ahmad M, Rees RC, Ali SA. Escape from immunotherapy: possible mechanisms that influence tumor regression/progression. Cancer Immunol Immunother 2004;53:844–54.
5. Staveley-O'Carrol K, Sotomayor E, Montgomery J, et al. Induction of antigen-specific T cell anergy: an early event in the cause of tumor progression. Proc Natl Acad Sci U S A 1998;95:1178–83.
6. Rosenberg SA, Yang JC, Restifo NP. Cancer immunotherapy: moving beyond current vaccines. Nat Med 2004;10:909–15.
7. Kaneda Y, Yamamoto S, Nakajima T. Development of HVJ envelope vector and its application to gene therapy. Adv Genet 2005;53PA:307–32.

8. Kaneda Y. New vector innovation for drug delivery: development of fusigenic non-viral particles. Curr Drug Targets 2003;4:599–602.
9. Kaneda Y, Nakajima T, Nishikawa T, et al. Hemagglutinating virus of Japan (HVJ) envelope vector as a versatile gene delivery system. Mol Ther 2002;6:219–26.
10. Ito M, Yamamoto S, Nimura K, Hiraoka K, Tamai K, Kaneda Y. Rad51 siRNA delivered by HVJ envelope vector enhances the anti-cancer effect of cisplatin. J Gene Med 2005;7:1044–52.
11. Yamano T, Kaneda Y, Huang S, Hiramatsu SH, Hoon DS. Enhancement of immunity by a DNA melanoma vaccine against TRP2 with CCL21 as an adjuvant. Mol Ther 2006;13:194–202.
12. Hiraoka K, Yamamoto S, Otsuru S, et al. Enhanced tumor-specific long-term immunity of hemagglutinating virus of Japan-mediated dendritic cell-tumor fused cell vaccination by coadministration with CpG oligodeoxynucleotides. J Immunol 2004;173:4297–307.
13. Mima H, Yamamoto S, Ito M, et al. Targeted chemotherapy against intraperitoneally disseminated colon carcinoma using a cationized gelatin-conjugated HVJ envelope vector. Mol Cancer Ther 2006;5:1021–8.
14. Worgall S, Busch A, Rivara M, et al. Modification to Capsid of the Adenovirus vector that enhances dendritic cell infection and transgene-specific cellular immune responses. J Virol 2004;78:2572–80.
15. Kaufman HL, DeRaffele G, Mitcham J, et al. Targeting the local tumor microenvironment with vaccinia virus expressing B7.1 for the treatment of melanoma. J Clin Invest 2005;115:1903–12.
16. Bristol JA, Zhu M, Ji H, et al. *In vitro* and *in vivo* activities of an oncolytic adenoviral vector designed to express GM-CSF. Mol Ther 2003;7:755–64.
17. Dasgupta S, Bhattacharya-Chatterjee M, O'Malley BW, Jr., et al. Recombinant vaccinia virus expressing interleukin-2 invokes anti-tumor cellular immunity in an orthotopic murine model of head and neck squamous cell carcinoma. Mol Ther 2006;13:183–93.
18. Leitner WW, Hwang LN, deVeer MJ, et al. Alphavirus-based DNA vaccine breaks immunological tolerance by activating innate antiviral pathways. Nat Med 2003;9:33–9.
19. Lu W, Zheng S, Li XF, Huang JJ, Zheng X, Li Z. Intratumor injection of H101, a recombinant adenovirus, in combination with chemotherapy in patients with advanced cancers: a pilot phase II clinical trial. World J Gastroenterol 2004;10:3634–8.
20. Bosma MJ, Carroll AM. The SCID mouse: definition, characterization, and potential uses. Annu Rev Immunol 1991;9:323–50.
21. Akira S, Takeda K. Toll-like receptor signaling. Nat Rev Immunol 2004;4:499–511.
22. Yoneyama M, Kikuchi M, Natsukawa T, et al. The RNA helicase RIG-I has an essential function in double-strand RNA-induced innate antiviral responses. Nat Immunol 2004;5:730–7.
23. Maloy KJ, Powrie F. Regulatory T cells in the control of immune pathology. Nat Immunol 2001;2:816–22.
24. Piccirillo CA, Shevach EM. Cutting edge: control of $CD8^+$ T cell activation by $CD4^+CD25^+$ immunoregulatory cells. J Immunol 2001;167:1137–40.
25. Sakaguchi S. Naturally arising Foxp3-expressing $CD25^+CD4^+$ regulatory T cells in immunological tolerance to self and non-self. Nat Immunol 2005;6:345–52.
26. Shevach EM. Regulatory T cells in autoimmunity. Annu Rev Immunol 2000;18:423–49.
27. Pasare C, Medzhitov R. Toll pathway-dependent blockade of $CD4^+CD25^+$ T cell-mediated suppression by dendritic cells. Science 2003;299:1033–6.
28. Doganci A, Eigenbrod T, Krung N, et al. The IL-6R α chain controls lung $CD4^+CD25^+$ Treg development and function during allergic airway inflammation *in vivo*. J Clin Invest 2005;115:313–25.
29. Liyanage UK, Moore TT, Joo HG, et al. Prevalence of regulatory T cells is increased in peripheral blood and tumor microenvironment of patients with pancreas or breast adenocarcinoma. J Immunol 2002;169:2756–61.
30. Wolf AM, Wolf D, Steurer M, Gastl G, Gunsilius E, Grubeck-Loebenstein B. increase of regulatory T cells in the peripheral blood of cancer patients. Clin Cancer Res 2003;9:606–12.
31. Sasada T, Kimura M, Yoshida Y, Kanai M, Takabayashi A. $CD4^+CD25^+$ regulatory T cells in patients with gastrointestinal malignancies: possible involvement of regulatory T cells in disease progression. Cancer 2003; 98:1089–99.
32. Woo EY, Chu CS, Goletz TJ, et al. Regulatory CD4(+)CD25(+) T cells in tumors from patients with early-stage non-small cell lung cancer and late-stage ovarian cancer. Cancer Res 2001;61:4766–72.
33. Curiel TJ, Coukos G, Zou L, et al. Specific recruitment of regulatory T cells in ovarian carcinoma fosters immune privilege and predicts reduced survival. Nat Med 2004;10:942–9.
34. Yu P, Lee Y, Liu W, et al. Intratumor depletion of $CD4^+$ cells unmasks tumor immunogenicity leading to the rejection of late-stage tumors. J Exp Med 2005; 201:779–91.
35. Turk MJ, Guevara-Patino JA, Rizzuto GA, Engelhorn ME, Sakaguchi S, Houghton AN. Concomitant tumor immunity to a poorly immunogenic melanoma is prevented by regulatory T cells. J Exp Med 2004;200: 771–82.
36. Ghiringhelli F, Puig PE, Roux S, et al. Tumor cells convert immature myeloid dendritic cells into TGF-β-secreting cells inducing $CD4^+CD25^+$ regulatory T cell proliferation. J Exp Med 2005;202:919–29.
37. Hirano T, Yasukawa K, Harada H, et al. Complementary DNA for a novel human interleukin (BSF-2) that induces B lymphocytes to produce immunoglobulin. Nature 1986;324:73–6.
38. Teranishi T, Hirano T, Arima N, Onoue K. Human helper T cell factor(s) (ThF). II. Induction of IgG production in B lymphoblastoid cell lines and identification of T cell replacing factor (TRF)-like factor(s). J Immunol 1982;128:1903–8.
39. Hirano T. Interleukin 6 and its receptor. Ten years later. Int Rev Immunol 1998;16:249–84.
40. Detournay O, Mazouz N, Goldman M, Tourgouz M. IL-6 produced by type I IFN DC controls IFN-γ production by regulating the suppressive effect of $CD4^+$ $CD25^+$ regulatory T cells. Hum Immunol 2005;66: 460–8.
41. Lopez CB, Garcia-Sastre A, Williams BR, Moran TM. Type I interferon induction pathway, but not released interferon, participates in the maturation of dendritic cells induced by negative-strand RNA viruses. J Infect Dis 2003;187:1126–36.
42. Lopez CB, Moltedo B, Alexopoulou L, Flavell RA, Moran TM. TLR-independent induction of dendritic cell maturation and adaptive immunity by negative-strand RNA virus. J Immunol 2004;173:6882–9.
43. Ito T, Amakawa R, Inaba M, et al. Plasmacytoid dendritic cells regulate Th cell responses through OX40 ligand and type I IFNs. J Immunol 2004;172: 4253–9.
44. Kaneda Y, Yamamoto S, Nakajima T. Development of HVJ envelope vector and its application to gene therapy. In: Huang L, Hung MC, Wagner E, editors. Non-viral vectors for gene therapy. London: Elsevier Academic Press; 2005. p. 307–32.

THE JOURNAL OF GENE MEDICINE
J Gene Med 2007; **9**: 55–62.
Published online 6 December 2006 in Wiley InterScience (www.interscience.wiley.com) **DOI:** 10.1002/jgm.989

RESEARCH ARTICLE

Rapid transport of plasmid DNA into the nucleolus via actin depolymerization using the HVJ envelope vector

Saroj Suvanasuthi
Katsuto Tamai
Yasufumi Kaneda*

Division of Gene Therapy Science, Graduate School of Medicine, Osaka University, 2-2 Yamada-oka, Suita, Osaka 565-0871, Japan

*Correspondence to:
Yasufumi Kaneda, Division of Gene Therapy Science, Graduate School of Medicine, Osaka University, 2-2 Yamada-oka, Suita, Osaka 565-0871, Japan.
E-mail:
kaneday@gts.med.osaka-u.ac.jp

Received: 28 April 2006
Revised: 9 October 2006
Accepted: 10 October 2006

Abstract

Background Although nuclear transport of therapeutic genes is an essential requirement of human gene therapy, factors required for nuclear entry of DNA remain to be elucidated. Non-viral vector systems have led to numerous improvements in the efficiency of delivery of exogenous DNA into cells. However, nuclear transport of plasmid is difficult to achieve.

Methods We examined nuclear translocation efficiency of Cy3-labeled plasmid DNA (Cy3-pDNA) delivered by the hemagglutinating virus of Japan envelope (HVJ-E) vector, Lipofectamine or microinjection. We also examined the effect of actin depolymerization on nuclear transport of Cy3-pDNA.

Results Cy3-pDNA reached the nucleus, particularly in the nucleolus, in 30 min after fusion-mediated delivery using the HVJ-E vector, while the DNA was retained in the cytoplasm during the observed period after the delivery by cationic liposomes. HVJ-E treatment transiently depolymerized actin filaments, and acceleration of nucleolar entry of microinjected DNA was achieved when treated with either empty HVJ-E or cytochalasin D, an inhibitor of actin depolymerization, prior to microinjection.

Conclusions These results suggest that plasmid DNA can be transported rapidly from the cytoplasm to the nucleolus when actin filaments are depolymerized. Thus, the HVJ-E vector can accelerate the transport of DNA to the nucleolus by actin depolymerization. Copyright © 2006 John Wiley & Sons, Ltd.

Keywords HVJ; plasmid DNA; nucleolus; actin; depolymerization

Introduction

Movement of DNA after its introduction into cells has been investigated since DNA transfer technology was first developed. Viral vectors have been widely used in gene therapy experiments since they possess the machinery for efficient delivery of exogenous DNA into cells [1,2]. Some viruses, such as adenovirus, SV40, HIV, and herpes virus, demonstrate rapid migration of their genomes into the nucleus even in non-dividing cells [3]. SV40 has viral capsid proteins that contain nuclear-localization sequences (NLSs) that trigger translocation of the virion to the nucleus and disassembly of the virion within the nucleus [4]. When adenovirus is taken up into cells by receptor-mediated endocytosis, virus escapes from the endosomes and

there is disassembly of the viral capsid, after which DNA-NLS-containing proteins are sorted in the nucleus [3,5]. HIV has an integrase required for nuclear migration of the viral genome [3]. The DNA-integrase complex, or pre-integration complex, common to oncoretroviruses, such as Moloney leukemia virus, cannot pass through the nuclear pore. Therefore, transgenes are not transported into the nuclei of non-dividing cells when oncoretroviral vectors are used [5]. Non-viral vector systems, on the other hand, have led to numerous improvements in the efficiency of delivery of exogenous DNA into cells [6,7]. Lipids, polymers, and fusion proteins enable successful DNA transfer to the cytoplasm. However, nuclear transport of plasmid is difficult to achieve [8]. When DNA was transferred to cells using a calcium phosphate precipitation method in the early days of DNA transfection, DNA was primarily observed in the perinuclear region, and the efficiency of nuclear translocation was generally only 1–2% of DNA levels observed in the cytoplasm [9]. Particularly within non-dividing cells, minimal translocation of DNA into the nucleus was observed after introduction into the cytoplasm [8]. Disruption of the nuclear envelope is required for efficient transfer of DNA into the nucleus [10]. Although a number of trials have reported nuclear transport of exogenous DNA using non-viral vectors, the results remain controversial. Both DNA nanoparticles compacted with Cys-Lys_{10} peptide [11] and Lipofectin/integrin-targeting peptide/plasmid DNA complex [12] succeeded in gene expression in post-mitotic cells or non-dividing cells. It is suggested that the DNA may transverse the nuclear envelope.

However, complexes containing plasmid DNA and nuclear proteins, such as histones, have been constructed; however, they do not enhance the nuclear migration of DNA [13,14]. On the other hand, NFkB p50-conjugated plasmid DNA is more rapidly transported into the nucleus than plasmid DNA alone [15]. Conjugation of a NLS peptide derived from SV40 with a luciferase gene fragment enhances luciferase gene expression by approximately 1000-fold, compared with the luciferase gene without the NLS peptide [16]. However, enhancement of green fluorescence protein (GFP) expression is not observed following conjugation of NLS peptide with GFP-plasmid DNA [17]. Non-classical NLS of heterogeneous nuclear ribonucleoprotein enhances the nuclear targeting of plasmid DNA delivered by lipofection [18,19]. A recent paper suggests that the nuclear migration of plasmid DNA might be sequence-dependent [20]. The SV40 enhancer sequence appears to facilitate nuclear migration of DNA by binding to transcription factors [21], which are transported to the nucleus by the Ran/importin system.

This data suggests that the machinery involved in active transport of nuclear proteins might also be involved in migration of DNA into the nucleus. However, the possibility of an inhibitory mechanism preventing movement of DNA into cells has not been investigated. Recently, it has been suggested that the actin cytoskeleton might be involved in DNA mobility in the cytoplasm and that actin filament disruption might enhance DNA mobility [22].

Actin depolymerization is induced by various compounds, such as botulinum C2 toxin, latrunculins, and cytochalasin D [23]. Human cytomegalovirus (CMV) induces actin depolymerization in the early stages of infection [24]. HVJ (hemagglutinating virus of Japan; Sendai virus) can also cause transient depolymerization of the actin cytoskeleton when membrane fusion between the virus and a cell occurs [25]. We developed a HVJ envelope (HVJ-E) vector, which enabled successful gene transfer and drug delivery in various cell lines *in vitro* (in cultured cells) and *in vivo* (in animal tissues or organs) through viral fusion activity [26]. Based on this evidence, we thus hypothesized that DNA might be more easily moved into cells when DNA is transferred using the HVJ-E vector.

Here we demonstrate the rapid transport of exogenous DNA into the nucleolus using the HVJ-E vector, which is dependent on depolymerization of the actin cytoskeleton.

Materials and methods

Labeling of plasmid DNA

A plasmid pGeneGrip vector (GTS, San Diego, CA, USA) was labeled with Cy3 fluorescence using a GeneGrip Cy3-PNA labeling kit (GTS), or with the Label IT® Cy™ 3 nucleic acid fluorescence labeling kit (Mirus Bio, Madison, USA) or with Cy3-labeled deoxy-CTP (Amersham Biosciences, Buckinghamshire, UK) using a terminal deoxynucleotidyl transferase (TaKaRa, Shiga, Japan), after linearization of the plasmid vector with a restriction endonuclease enzyme (KpnI in case of pGL3) leaving the 3′-end or blunt end of DNA.

Cell culture

HeLa cells and human primary fibroblast (FS3) cells were maintained in Dulbecco's modified Eagle's medium (DMEM) supplemented with 10% fetal calf serum (FCS) and penicillin/streptomycin mixed solution (Nakalai, Kyoto, Japan).

Microinjection of plasmid DNA

Cy3-pDNA was dissolved in calcium-free phosphate-buffered saline (PBS) at a concentration of 1 μg/ml pDNA, after which the pDNA solutions were centrifuged through a 0.22 μm filter. To verify intact nuclear envelopes of the injected cells, FITC-labeled 70-kDa dextran (Sigma, Steinheim, Germany) was co-injected with the pDNA. The injections were performed using a semi-automatic injection system (Transjector 5246; Eppendorf, Hamburg, Germany) attached to an Eppendorf micromanipulator

5171 mounted on an inverted microscope. Cytosolic microinjections were performed with a Z-depth limit option using glass micropipettes (Femtotips I; Eppendorf). The estimated volume of each injection was 0.3–0.5 picoliter (an estimation based on injection pressure and duration, according to the manufacturer's specifications). During injection, the cells were kept in DMEM supplemented with 10% FCS. The cells were washed with PBS and replaced with DMEM supplemented with 10% FCS after microinjection. To verify that nuclear envelopes of the injected cells remained intact during microinjection, FITC-labeled 70-kDa dextran, which cannot translocate through the nuclear pore complex, was introduced into the cytoplasm with each Cy3-pDNA solution, and only those cells capable of excluding dextran from the nucleus were used in the analysis, as previously described [15].

To evaluate the effects of cytochalasin D or HVJ-E on the movement of microinjected DNA, cytochalasin D (0.025 μg/ml; A.G. Scientific, CA, USA) or HVJ-E (3×10^9 particles) was added to cells for 30 min before or after microinjection, respectively.

Each experiment was repeated at least eight times, and approximately 20 cells were microinjected with Cy3-pDNA for each experiment.

Plasmid DNA delivery using HVJ-E

Aliquots of inactivated HVJ (3×10^{10} particles) were centrifuged (1500 rpm, 15 min) at 4 °C, after which the viral pellet was suspended in 15 μl protamine sulfate (1 mg/ml) and incubated on ice for 15 min. The viral suspension was then mixed with plasmid DNA (200 μg) with 3% Triton X-100. The mixture was centrifuged at 15 000 rpm for 5 min at 4 °C. After washing the pellet with 1 ml BSS to remove the detergent and unincorporated DNA, the HVJ-E vector containing pDNA was suspended in 300 μl PBS. Then, HeLa cells (1×10^6 cells/dish) were prepared 24 h before transfection. HVJ-E (3×10^9 particles) was mixed with protamine sulfate (100 μg/ml) and added to the HeLa cells cultured in DMEM without FCS. The DNA-tapping efficiency of the HVJ-E vector was approximately 15% [26]. Therefore, the final amount of pDNA transferred to cells using the HVJ-E vector was 3 μg/1×10^6 cells/dish. After 30 min of incubation at 37 °C under 5% CO_2, the medium was replaced by DMEM supplemented with 10% FCS, after which the cells were cultured at 37 °C under 5% CO_2 and photos were taken at various intervals.

Plasmid DNA delivery using Lipofectamine

DNA transfection was performed with HeLa cells in 35-mm glass-bottomed dishes (about 1×10^6 cells/dish prepared 24 h before transfection) by adding 5 μl of Lipofectamine (Invitrogen, CA, USA) transfection reagent mixed with 3 μg each of pDNA dissolved in DMEM without FCS. After 30 min of incubation at 37 °C under 5% CO_2, the medium was replaced by DMEM supplemented with 10% FCS and transfected cells were cultured at 37 °C under 5% CO_2, and photos were taken at various intervals.

Luciferase assay

HeLa cells were collected at various time points after HVJ-E-mediated or Lipofectamine-mediated transfection of the luciferase reporter plasmid, and suspended in 500 μl of cell culture lysis reagent. The cell lysate samples were then clarified by centrifugation at 10 000 *g* for 10 min at 4 °C, after which a volume of 20 μl of each supernatant was subjected to luciferase assay using the Promega luciferase assay system and a Lumat LB 9501 luminophotometer (Belthold, Wildbad, Germany), as previously described [26]. The protein content of the samples was measured using the DC protein assay (Bio-Rad, CA, USA)

In situ hybridization to detect transgene expression

HeLa cells were grown on cover glass slides 24 h before the experiment. After pGL3 transfection with HVJ-E, the cells were fixed with pre-warmed 4% paraformaldehyde in PBS for 20 min followed by permeabilization with 0.5% Triton X-100 in PBS for 5 min. Then, the cells were washed with PBS three times before adding a blocking solution (0.5% bovine serum albumin (BSA), 50 mM glycine, and 2% goat serum in PBS) to stop the permeabilizing process.

RNA probes were made using the DIG RNA labeling kit (Roche Applied Science, Mannheim, Germany). Digoxigenin-labeled RNA probes were generated from luciferase-pSPT18 plasmid by *in vitro* transcription with T7 and SP6 RNA polymerase respectively, for the antisense and sense probes.

The hybridization reaction was performed in an InsituPro (Intavis, CA, USA). Hybridization with digoxigenin-labeled riboprobes was done at 65 °C overnight in 50% deionized formamide, 1× NaCl, 1× Denhardt's solution, 10% dextran sulfate, and 250 μg/ml yeast RNA. The non-hybridized probe was removed by two washes with 2× SSC for 5 min each at room temperature, 2× SSC and 50% formamide at 65 °C for 30 min, followed by rinses with decreasing concentrations of SSC. Non-specific sites were blocked with 2% blocking reagent (Roche Applied Science) in 0.1 mol/l maleic acid, 0.15 mol/l NaCl, pH 7.5, 0.1% Tween 20, and 2% goat serum for 1 h at room temperature. Slides were incubated overnight at room temperature with alkaline phosphatase-conjugated polyclonal sheep anti-digoxigenin antibody (Roche Applied Science). The reaction product was visualized using nitroblue tetrazolium and 5-bromo-4-chloro-3-indolylphosphate (Roche Applied Science).

Confocal laser scanning microscopy

Fluorescent images were acquired with a Nikon eclipse TE2000-U microscope (Nikon, Japan) with a confocal laser scanning system (BioRad Radiance 2100, Hertfordshire, UK). At each time point, fluorescent images were collected using BioRad Laser sharp 2000 v 6.2 software.

Immunofluorescence experiments

Cells were grown on cover glass slides 24 h before the experiment. In some experiments, the cells were treated with HVJ-E (3×10^9 particles), or cytochalasin D (0.025 μg/ml).

To study the actin cytoskeleton, the cells were fixed with 37 °C pre-warmed 4% paraformaldehyde in PBS for 20 min. The cells were then permeabilized with 0.5% Triton X-100 in PBS for 5 min. The cells were then washed with PBS three times before adding a blocking solution (0.5% BSA, 50 mM glycine, and 2% goat serum in PBS) to stop the permeabilizing process, and Alexar Fluor 488 phalloidin (35 μl/1 ml) (Molecular Probes, Leiden, The Netherlands) was added to the incubation for 60 min. The cells were then washed six times with PBS. The cell nuclei were stained with Hoechst 33 342 (Molecular Probes).

To study the nuclear envelope and nuclear structure, HeLa cells were fixed with cold methanol for 5 min and then washed three times with PBS. FS3 cells were fixed with 37 °C pre-warmed 4% paraformaldehyde in PBS for 20 min and then permeabilized with 0.5% Triton X-100 in PBS for 5 min. The cells were then washed with PBS three times. After fixation both cell types were blocked with a blocking solution for 30 min before the addition of anti-upstream binding factor (UBF) (Santa Cruz Biotechnology, CA, USA) and anti-lamin B prepared in our laboratory [27] for staining of the nucleoli and nuclear envelope, respectively. Cells were incubated overnight at 4 °C, after which they were washed six times in PBS. FICT-labeled anti-IgG (Molecular Probes) was then added, followed by incubation for 1 h. The cells were then washed six times in PBS. The cell nuclei were stained with Hoechst 33 342.

All immunofluorescent images were taken using a confocal laser scanning microscope, as described above.

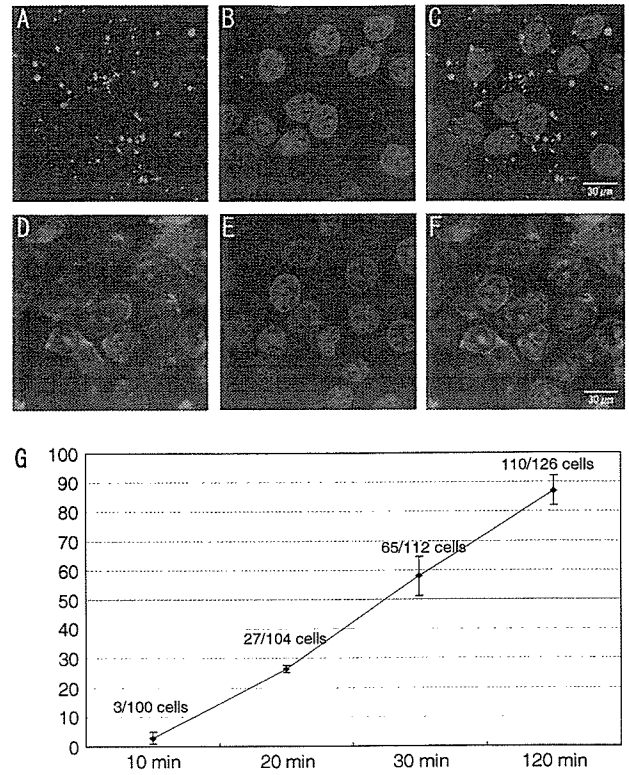

Figure 1. The localization of Cy3-pDNA, labeled with the Label IT® Cy™ 3 labeling kit (Mirus), was observed using confocal microscopy 120 min after the start of a 30 min incubation period of HeLa cells with Lipofectamine (A, B, C) or with HVJ-E vector (D, E, F) containing Cy3-pDNA. The localization of Cy3-pDNA (A, D), nuclei staining with Hoechst 33 258 (B, E) and the merged photo (C, F) was shown using confocal microscopy. Nucleolus-positive cells were counted (G) at 10 min, 20 min, 30 min and 120 min after the start of transfection of the HVJ-E vector containing Cy3-pDNA

Results

Characteristic rapid nuclear entry of plasmid DNA introduced by HVJ-E

First, we investigated localization of Cy3-labeled plasmid DNA (Cy3-pDNA) introduced into the cells by Lipofectamine (Figures 1A–1C) and by the HVJ-E vector (Figures 1D–1F) at 120 min after transduction. Lipofectamine-transduced plasmid DNA localized exclusively in the cytoplasm with a dot pattern (Figure 1A), while plasmid DNA transported by the HVJ-E vector located in the nucleus with characteristic particulate accumulation as well as in the cytoplasm with diffuse distribution. Then we performed a time-course analysis of localization of Cy3-labeled plasmid DNA (Cy3-pDNA) introduced directly into the cytoplasm of HeLa cells using the HVJ-E vector. Statistical analysis indicated that 26% of the HVJ-E-transduced cells showed nuclear accumulation of the plasmid DNA at 20 min post-transduction, and this ratio rapidly increased to 87% in 120 min (Figure 1G). To investigate the specific focus of HVJ-E-introduced pDNA in the nucleus, we then examined the location of Cy3-pDNA relative to the nucleoli. Immunofluorescent analysis using antibody against UBF, which is a nucleoli-specific protein complex, revealed co-localization of UBF with HVJ-E-mediated Cy3-pDNA in the nucleus (Figures 2A–2D). Rapid migration of Cy3-pDNA into the nucleolus was also observed when human primary fibroblast cells were transfected with the HVJ-E vector, and the localization of fluorescent DNA was not changed by different DNA labeling methods (Figures 2E–2H). Next, we examined whether gene expression was achieved from DNA introduced using a HVJ-E vector. To test the possibility, *in situ* hybridization

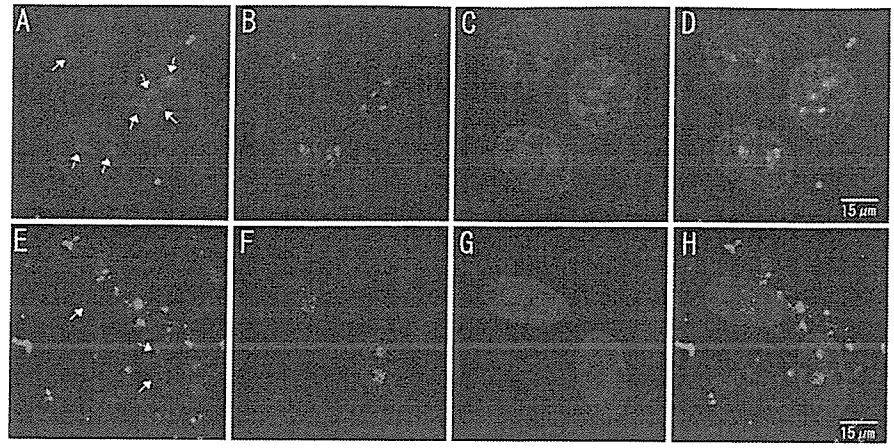

Figure 2. HeLa cells (A–D) and FS3 cells (E–H) transfected with the HVJ-E vector containing Cy3-pDNA were fixed with cold methanol or 4% paraformadehyde and stained with anti-UBF protein antibody, followed by FITC-labeled anti-mouse IgG. The localization of Cy3-pDNA, labeled with the Label IT® Cy™ 3 labeling kit (Mirus) (A, E), and UBF (B, F) was observed using confocal microscopy. The nuclei were stained with Hoechst 33 258 (C, G). The merged photo is also presented (D, H)

to detect luciferase mRNA was done at various intervals after HVJ-E-containing pGl3 luciferase gene transfection (Figures 3A–3F). By antisense probe which was generated by T7 RNA polymerase, the data showed the ratio of luciferase RNA-positive cells was 4.9, 51.4 and 82.4% at 2, 4 and 24 h post-transfection. The luciferase activity was also measured at various time points after delivery of the luciferase expression plasmid by a HVJ-E vector (Figure 3G). These data indicate that HVJ-E-mediated delivery produced rapid transport of plasmid DNA into the nucleus, particularly the nucleolus, with induction of gene expression.

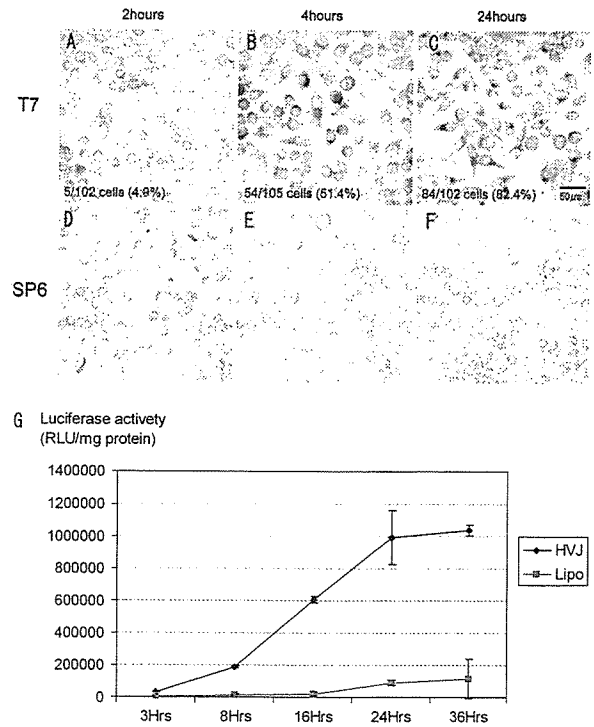

Figure 3. *In situ* hybridization to detect luciferase mRNA was performed at 2 h (A, D), 4 h (B, E) and 24 h (F, G) after transfection with HVJ-E containing pCMV-luciferase. Antisense and sense Dig-labeled RNA probes were generated from luciferase-pSPT18 plasmid with T7 (A–C) or SP6 (D–F) RNA polymerase, respectively. The reaction product was visualized using nitroblue tetrazolium and 5-bromo-4-chloro-3-indolylphosphate. Luciferase gene expression was assessed 3, 8, 16, 24 and 36 h after transfection with HVJ-E containing pCMV-luciferase (H)

Effect of HVJ-E treatment on nucleolar entry of microinjected plasmid DNA

Next, we compared the localization of Cy3-pDNA following microinjection alone, with that observed after microinjection and HVJ treatment.

By microinjection alone, Cy3-pDNA was present only in the cytoplasm until 240 min after injection (Figures 4A–4D), and, thus, was not confined to the nucleolus. However, following treatment with empty HVJ-E after microinjection, fluorescence of Cy3-pDNA was primarily observed in the cytoplasm, after which fluorescence became apparent in the nucleus at 30 min, and much clearer at 120 min after injection (white arrow, Figures 4I–4L). This fluorescence was confined to particulate structures, not diffusely present in the nucleoplasm. The particulate structures were determined to be nucleoli, as shown in Figure 2. However, co-injected FITC-labeled dextran was retained in the cytoplasm and green fluorescence of FITC-labeled dextran was not detected in either the nucleoplasm or the nucleolus (Figures 4E–4H and 4M–4P).

Transient depolymerization of actin filaments with HVJ-E treatment

Since recent reports have indicated that the actin cytoskeleton plays a significant role in limiting DNA mobility in the cytoplasm [23], we examined the assembly

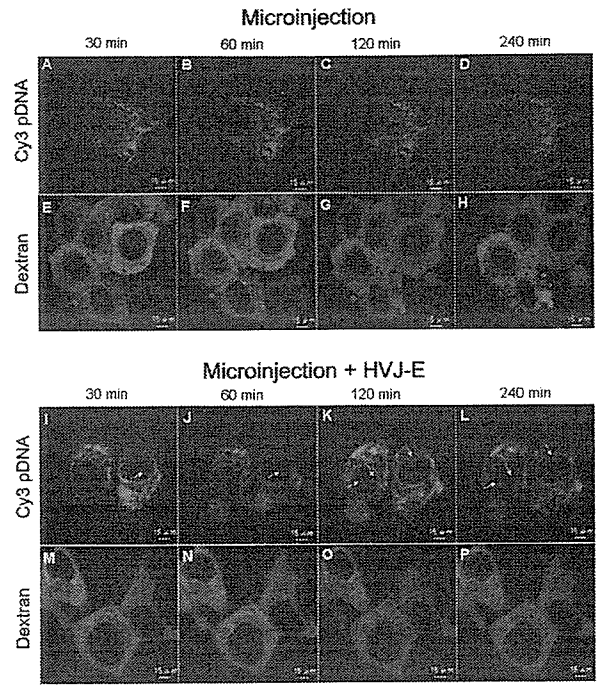

Figure 4. The localization of Cy3-pDNA labeled with the GeneGrip Cy3-PNA labeling kit (GTS) was observed using confocal microscopy 30, 60, 120 and 240 min after injection of DNA into the cytoplasm of HeLa cells by microinjection alone (A–D), or microinjection with HVJ-E treatment (I–L). The white arrow indicates Cy3-pDNA in the nucleus of the cells. The HVJ-E vector was removed by changing the medium 30 min after microinjection. The localization of co-injected FITC-labeled dextran with or without HVJ-E treatment was analyzed (E–H and M–P)

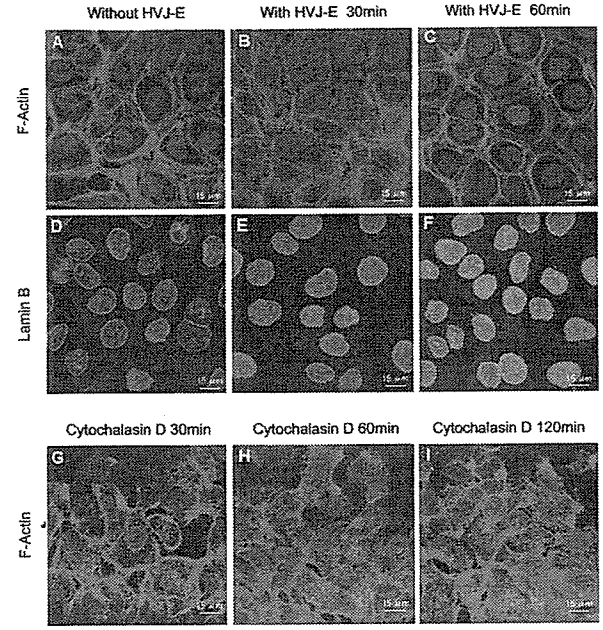

Figure 5. HeLa cells on a glass slide were treated with empty HVJ-E vector (3×10^9 particles), and the HVJ-E vector was removed after 30 min. Then, the actin filaments were stained with Alexar Fluor 488 phalloidin at 0 and 30 min after the removal of HVJ-E. To detect nuclear envelope protein, cells fixed with cold methanol were treated with anti-lamin B antibody, followed by treatment with FITC-labeled anti-rabbit IgG (D–F). Actin and lamin B were observed before (A, D) or 30 (B, E) and 60 (C, F) min after the start of a 30 min incubation period with HVJ-E. In another experiment, HeLa cells were treated with cytochalasin D at a concentration of 0.025 μg/ml for 30 (G), 60 (H) and 120 (I) min. The actin cytoskeleton and nuclei were stained as described above

of actin filaments in HeLa cells before and after HVJ-E treatment. As demonstrated in Figure 5, depolymerization of actin filaments was clearly observed immediately after the removal of HVJ-E treatment (Figure 5B), and re-polymerization of actin was observed 30 min after the removal of HVJ-E in culture (Figure 5C). On the other hand, HVJ-E treatment did not significantly alter the structure of lamin B of the nuclear envelope of HeLa cells (Figures 5D–5F), indicating rather a specific effect of HVJ-E on disassembly of the actin cytoskeleton.

Similar depolymerization of actin is known to result from treatment with cytochalasin D (0.025 μg/ml). We attempted to determine the particular conditions required for actin depolymerization within HeLa cells as a result of treatment with cytochalasin D, and determined that sufficient actin depolymerization was induced by 60 min of incubation with cytochalasin D at a concentration of 0.025 μg/ml (Figure 5H).

Increased nucleolar entry of plasmid DNA by actin depolymerization

We then evaluated the effect of cytochalasin D on the nuclear entry of plasmid DNA introduced by microinjection. Cytochalasin D was added to the culture medium 30 min prior to microinjection of Cy3-pDNA into the cytoplasm of HeLa cells, after which the time-dependent nuclear entry of injected Cy3-pDNA was evaluated at the time points indicated in Figure 6. With cytochalasin D treatment, Cy3-pDNA started to accumulate in the nucleus 60 min after microinjection (Figure 6C), revealing a significant acceleration of nuclear entry, compared to the rate of nuclear entry observed after microinjection of Cy3-pDNA in the absence of cytochalasin D (Figure 4B). Nuclear Cy3-pDNA was localized to the nucleolus by indirect immunofluorescence, as shown in Figure 1 (data not shown). With cytochalasin D, Cy3-pDNA remained in the nucleolus at 120 and 240 min after microinjection (Figures 6D and 6E). Co-injected FITC-labeled dextran was not transported into the nucleus and remained in the cytoplasm, as presented in Figure 4.

These results suggest that the actin cytoskeleton can inhibit the movement of pDNA in the cytoplasm, and that depolymerization of the actin cytoskeleton can enhance translocation of pDNA to the nucleolus.

Discussion

We have demonstrated that plasmid DNA delivered by the HVJ-E vector rapidly reaches the nucleolus by inducing depolymerization of the actin cytoskeleton.

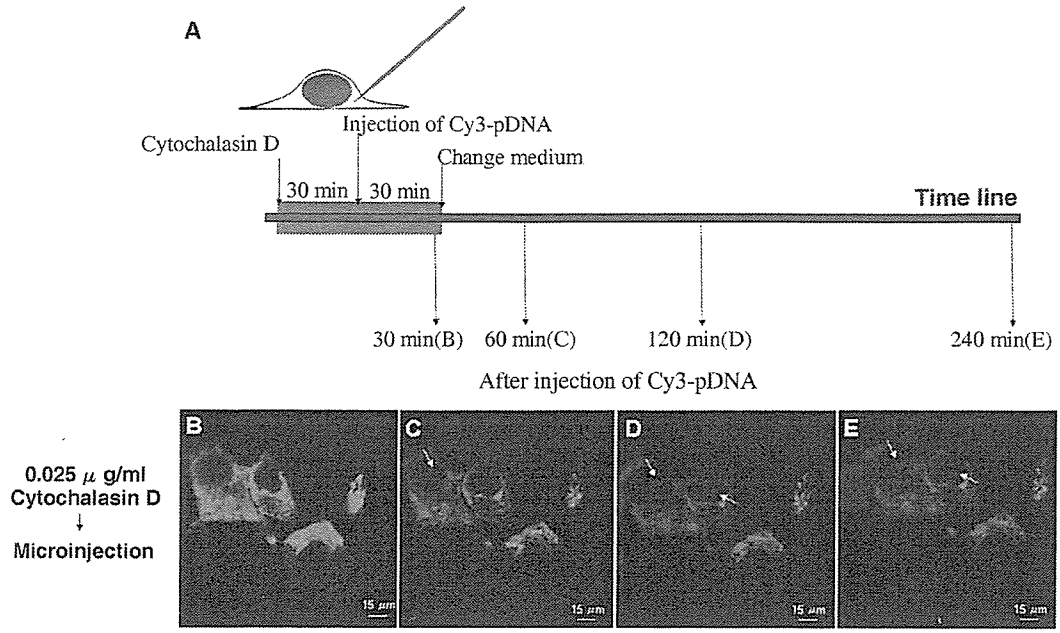

Figure 6. As illustrated, cytochalasin D was first added to HeLa cells at a concentration of 0.025 μg/ml, and Cy3-pDNA labeled with the GeneGrip Cy3-PNA label kit (GTS) was microinjected 30 min later (A). Cytochalasin D was removed 30 min after microinjection by replacement of the medium. The localization of Cy3-pDNA was observed using confocal microscopy 30 (B), 60 (C), 120 (D) and 240 (E) min after the injection of Cy3-pDNA

The HVJ-E vector delivers plasmid DNA by membrane fusion, and induces gene expression in cultured cells and tissue [28]. Indeed, using the HVJ-E vector, expression of the human HGF gene was detected in non-dividing neuronal cells of a spiral ganglion of the inner ear [29]. Although this indicates that plasmid DNA delivered by the HVJ-E vector is translocated into the nucleus, the mechanism by which this occurs remains unclear. Our present results suggest that the expression of plasmid DNA in neuronal cells of a spiral ganglion of the inner ear results from rapid transport of the DNA into the nucleolus by the HVJ-E vector. Luciferase gene expression was achieved when DNA delivered into the nucleus became primarily located in the nucleolus. It is difficult to exclude the possibility that a small amount of DNA remained in the nucleoplasm. However, when trichostatin, an inhibitor of histone deacetylase, was added to HeLa cells after DNA delivery using the HVJ-E vector, luciferase gene expression was approximately 10-fold of that achieved in the absence of inhibitor as previously reported [30–32]. DNA localization was not altered by the presence of trichostatin. Nuclear fluorescence was primarily observed in the nucleolus. This suggests that, although the nucleolus is where ribosomal RNA genes are transcribed, transcription of the luciferase gene under control of the CMV promoter might occur in the nucleolus following delivery by the HVJ-E vector (Figure 1).

Following microinjection using a micropipette, most of the DNA was retained in the cytoplasm until 4 h after injection and no significant fluorescence was seen in the nucleus (Figure 4). This DNA was found in the nucleoplasm, and not confined to the nucleolus. The mobility of the microinjected DNA was much slower than that observed following introduction by the HVJ-E vector. However, some of the microinjected DNA was transported into the nucleus following HVJ-E treatment after microinjection, and localization was then confined to the nucleolus, not the nucleoplasm. On occasion, Cy3-pDNA was detected more rapidly throughout the nucleoplasm after microinjection. In such cases, co-injected FITC-dextran was also seen in the nucleoplasm, suggesting that the nuclear envelope may have been damaged, thus losing its transport selectivity during the microinjection procedure. Therefore, it is likely that the microinjected DNA could be transported into the nucleolus with HVJ-E treatment as long as the nuclear envelope remains intact.

HVJ induced transient actin depolymerization, as shown in Figure 5. Cytochalasin D, which induced actin filament depolymerization, also enhanced the transport of DNA into the nucleolus after microinjection (Figure 6). We concluded that depolymerization of the actin cytoskeleton induced the transport of plasmid DNA into the nucleolus. Dauty *et al.* found that the integrity of the actin cytoskeleton determined the mobility of DNA in the cytoplasm [23]. This finding is consistent with the present results; however, they did not examine the nuclear transport of DNA with regard to actin depolymerization. Therefore, a route to transport plasmid DNA into the nucleolus after actin depolymerization may exist. It is possible that this movement is specific for plasmid DNA lacking a NLS. When dextran without a NLS was microinjected into the cytoplasm, dextran was retained in the cytoplasm, even with HVJ-E treatment. In an experiment in which DNA was conjugated with

a NLS-containing protein, p50 of NFkB, followed by microinjection into the cytoplasm of HeLa cells [15], DNA reached the nucleus and was localized within the nucleoplasm, not the nucleolus. Thus, it is thought that some molecules, such as DNA, may be transported into the nucleolus in the absence of NLS when the actin cytoskeleton is depolymerized, although the mechanism by which this occurs is still unclear. However, DNA delivered by the HVJ-E vector moved into the nucleolus more effectively, compared with following microinjection, even when the cells were treated with cytochalasin D or empty HVJ-E vector after microinjection. Therefore, it is likely that the HVJ-E vector may have an additional enhancing effect with regard to movement of DNA into the nucleolus.

We thus found that HVJ can produce transient actin depolymerization in the initial stages of infection; however, the biological significance of actin depolymerization in the initial stages of infection remains unclear. Based on our results, actin depolymerization might enhance mobility of the viral RNA genome within the cytoplasm, thus enabling efficient replication of the viral genome and translation of viral proteins in infected cells.

The HVJ-E vector can deliver genes directly to the cytoplasm by membrane fusion [30], which avoids degradation of exogenous genes [32]. Another advantage is that the vector can achieve rapid transfer of DNA into the nucleus, thus overcoming a significant obstacle of using non-viral gene delivery vectors, thereby inducing efficient gene expression *in vivo*.

References

1. Mulligan RC. The basic science of gene therapy. *Science* 1993; **260**: 926–932.
2. Verma IM, Weizmann MD. Gene therapy: twenty-first century medicine. *Annu Rev Biochem* 2005; **74**: 711–738.
3. Izaurralde E, Kann M, Pante N, Sodeik B, Hohn T. Viruses, microorganisms and scientists meet the nuclear pore, Leysin, VD, Switzerland, February 26–March 1, 1998. *EMBO J* 1999; **18**: 289–296.
4. Greber UF, Kasamatsu H. Nuclear targeting of SV40 and adenovirus. *Trends Cell Biol* 1996; **6**: 189–195.
5. Greber UF, Suomalainen M, Stidwill RP, Boucke K, Ebersold MW, Helenius A. The role of the nuclear pore complex in adenovirus DNA entry. *EMBO J* 1997; **16**: 5998–6007.
6. Ledley FD. Nonviral gene therapy: the promise of genes as pharmaceutical products. *Hum Gene Ther* 1995; **6**: 1129–1144.
7. Conwell CC, Huang L. Recent advances in non-viral gene delivery. *Adv Genet* 2005; **53**: 1–18.
8. Zabner J, Fasbender AJ, Moninger T, Poellinger KA, Welsh MJ. Cellular and molecular barriers to gene transfer by a cationic lipid. *J Biol Chem* 1995; **270**: 18997–19007.
9. Loyter A, Scangos GA, Ruddle FH. Mechanisms of DNA uptake by mammalian cells: fate of exogenously added DNA monitored by the use of fluorescent dyes. *Proc Natl Acad Sci U S A* 1982; **79**: 422–426.
10. Brunner S, Sauer T, Carotta S, Cotton M, Saltik M, Wagner E. Cell cycle dependence of gene transfer by lipoplex, polyplex and recombinant adenovirus. *Gene Ther* 2000; **7**: 401–407.
11. Liu G, Li D, Pasumarthy MK, *et al.* Nanoparticles of compacted DNA transfect postmitotic cells. *J Biol Chem* 2003; **278**: 32578–32586.
12. Meng QH, Robinson D, Jenkins RG, McAnulty RJ, Hart SL. Efficient transfection of non-proliferating human airway epithelial cells with a synthetic vector system. *J Gene Med* 2004; **6**: 210–221.
13. Fritz JD, Herweijer H, Zhang G, Wolff JA. Gene transfer into mammalian cells using histone-condensed plasmid DNA. *Hum Gene Ther* 1996; **7**: 1395–1404.
14. Sebestyen MG, Ludtke JJ, Bassik MC, *et al.* DNA vector chemistry: the covalent attachment of signal peptides to plasmid DNA. *Nat. Biotechnol* 1998; **16**: 80–85.
15. Meskia A, Kiss V, Brumfeld V, Ghosh G, Reich Z. Enhanced intracellular mobility and nuclear accumulation of DNA plasmids associated with a karyophilic protein. *Hum Gene Ther* 2005; **16**: 200–208.
16. Zanta MA, Belguise-Valladier P, Behr JP. Gene delivery: a single nuclear localization signal peptide is sufficient to carry DNA to the cell nucleus. *Proc Natl Acad Sci U S A* 1999; **96**: 91–96.
17. Tanimoto M, Kamiya H, Minakawa N, Matsuda A, Harashima H. No enhancement of nuclear entry by direct conjugation of a nuclear localization signal peptide to linearized DNA. *Bioconjugate Chem* 2003; **14**: 1197–1202.
18. Subramanian A, Ranganathan P, Diamond SL. Nuclear targeting peptide scaffolds for lipofection of nondividing mammalian cells. *Nat Biotechnol* 1999; **17**: 873–877.
19. Ma H, Zhu J, Maronski M, *et al.* Non-classical nuclear localization signal peptides for high efficiency lipofection of primary neurons and neuronal cell lines. *Neuroscience* 2002; **12**: 1–5.
20. Dean DA. Import of plasmid DNA into the nucleus is sequence specific. *Exp Cell Res* 1997; **230**: 293–302.
21. Wilson GL, Dean BS, Wang G, Dean DA. Nuclear import of plasmid DNA in digitonin-permeabilized cells requires both cytoplasmic factors and specific DNA sequences. *J Biol Chem* 1999; **274**: 22025–22032.
22. Val derrama F, Duran JM, Babia T, Barth H, Renau-Piqueras J, Egea G. Actin microfilaments facilitate the retrograde transport from the Golgi complex to the endoplasmic reticulum in mammalian cells. *Traffic* 2001; **2**: 717–726.
23. Dauty E, Verkman AS. Actin cytoskeleton as the principal determinant of size-dependent DNA mobility in cytoplasm. *J Biol Chem* 2005; **280**: 7823–7828.
24. Jones NL, Lewis JC, Kilpatrick BA. Cytoskeletal disruption during human cytomegalovirus infection of human lung fibroblasts. *Eur J Cell Biol* 1986; **41**: 304–312.
25. Okada Y. Sendai virus-induced cell fusion. *Methods Enzymol* 1993; **221**: 18–41.
26. Kaneda Y, Nakajima T, Nishikawa T, *et al.* Hemagglutinating virus of Japan (HVJ) envelope vector as a versatile gene delivery system. *Mol Ther* 2002; **6**: 219–226.
27. Kaneda Y, Kinoshita K, Sato M, Tanaka K, Kaneda Y. The analysis of 40 kDa nuclear protein, p40, in interphase cells and mitotic cells. *J Cell Sci* 1993; **106**: 741–748.
28. Kaneda Y, Yamamoto S, Nakajima T. Development of HVJ envelope vector and its application to gene therapy. In *Non-viral Vectors for Gene Therapy*, Huang L, Hung M-C, Wagner E (eds). Elsevier Academic Press: 2005; 307–332.
29. Oshima K, Shimamura M, Mizuno S, *et al.* Intrathecal injection of HVJ-E containing HGF gene to cerebrospinal fluid can prevent and ameliorate hearing impairment in rats. *FASEB J* 2004; **18**: 212–214.
30. Chen WY, Bailey EC, McCune SL, Dong JY, Townes TM. Reactivation of silenced, virally transduced genes by inhibitors of histone deacetylase. *Proc Natl Acad Sci U S A* 1997; **94**: 5798–5803.
31. Dion LD, Goldsmith KT, Tang DC, Engler JA, Yoshida M, Garver RI Jr. Amplification of recombinant adenoviral transgene products occurs by inhibition of histone deacetylase. *Virology* 1997; **231**: 201–209.
32. Nakamura N, Hart DA, Frank CB, *et al.* Efficient transfer of intact oligonucleotides into the nucleus of ligament scar fibroblasts by HVJ-cationic liposomes is correlated with effective antisense gene inhibition. *J Biochem* 2001; **129**: 755–759.

J Mol Med
DOI 10.1007/s00109-006-0120-y

ORIGINAL ARTICLE

Needleless intranasal administration of HVJ-E containing allergen attenuates experimental allergic rhinitis

Eri Yasuoka · Kazuo Oshima · Katsuto Tamai · Takeshi Kubo · Yasufumi Kaneda

Received: 13 July 2006 / Revised: 13 September 2006 / Accepted: 22 September 2006

Abstract Allergic rhinitis (AR) is one of the most common chronic diseases. Although current medications are highly effective in controlling its symptoms, they do not reverse the allergen-specific hypersensitivities that underlie the disease. Immunoglobulin E is a key mediator of AR, and preventing its production is clinically important. In this study, we developed an efficient needleless intranasal protein delivery system using the hemagglutinating virus of Japan envelope vector (HVJ-E). Intranasal delivery of ovalbumin (OVA) once a week for 3 weeks using this system enhanced OVA-induced interferon-γ production by murine splenocytes. This treatment also attenuated the OVA-induced release interleukin-4 (IL-4) and IL-5 from splenocytes and the production of plasma OVA-specific immunoglobulin E in OVA-sensitive AR model mice. Thus, allergen-containing HVJ-E may be useful for noninvasive treatment of AR.

Keywords Hemagglutinating virus of Japan envelope vector · Allergic rhinitis · Ovalbumin · Th1/Th2 balance · Immunoglobulin E

Abbreviations

AR	allergic rhinitis
HVJ-E	hemagglutinating virus of Japan envelope vector
OVA	ovalbumin

E. Yasuoka · K. Tamai · Y. Kaneda (✉)
Department of Gene Therapy Science,
Graduate School of Medicine, Osaka University,
2-2 Yamadaoka,
Suita, Osaka 565-0871, Japan
e-mail: kaneday@gts.med.osaka-u.ac.jp

E. Yasuoka · K. Oshima · T. Kubo
Department of Otolaryngology, Graduate School of Medicine,
Osaka University,
Suita, Osaka, Japan

ERI YASUOKA
studied medicine at Osaka University and is presently a student of Graduate School of Medicine of Osaka University in Osaka, Japan. Her research interests focus on allergic disease.

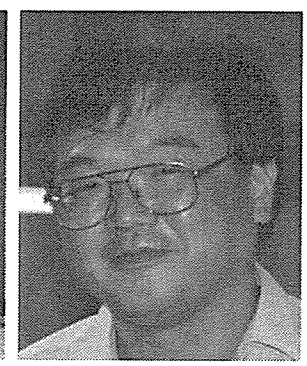

YASUFUMI KANEDA
obtained his M.D. and Ph.D. from Osaka University and is currently a professor at Department of Gene Therapy Science, Graduate School of Medicine, Osaka University in Osaka, Japan. His research interests include vector development, gene discovery, gene expression, cardiovascular gene therapy and anticancer therapy.

Introduction

Allergic rhinitis (AR) is one of the most common forms of atopic disease and has an estimated prevalence ranging from 5 to 22% [1, 2]. Prevalence estimates suggest that, in developed countries, seasonal and perennial AR occurs in 10% and 10–20% of the population, respectively. Furthermore, for children, the prevalence of AR may be as high as 40% [1], and it seems to be becoming more common. Thus,

AR is one of the most common chronic diseases in the industrialized world. Unfortunately, although there are effective medications for treating the symptoms, the current medications do not reverse allergen-specific hypersensitivities and are therefore only palliative and often must be used daily for years.

Type I allergies, such as AR, are characterized by an increase in the production of immunoglobulin E (IgE) and by mast cell degranulation, which releases histamine and other allergic mediators [3]. Clinical observations have suggested a correlation between serum IgE levels and the extent or the severity of AR. Antigen-specific binding of IgE on mast cell Fc^{ε} receptors induces receptor cross-linking and the release of inflammatory mediators, such as histamine, leukotrienes, and prostaglandins. Recent studies have shown that the binding of IgE itself to Fc^{ε} receptors in the absence of allergen can stimulate the release of inflammatory mediators from mast cells [4, 5]. Hence, the inhibition of IgE production is an important therapeutic target for the prevention of AR.

IgE production by plasma cells is regulated by antigen-specific $CD4^+$ T cells [6, 7]. Naive $CD4^+$ T cells stimulated with allergen in the presence of interleukin-4 (IL-4) express GATA-3, a member of the GATA family of transcription factors, and differentiate into Th2 cells, which secrete cytokines such as IL-4, IL-5, and IL-13 [8]. On the other hand, naive $CD4^+$ T cells stimulated with allergen in the presence of IL-12 express T bet, a T-box family of transcription factor, and preferentially differentiate into Th1 cells, which secrete cytokines such as IL-2 and interferon-γ (IFN-γ) [9]. Furthermore, Th1 or Th2 effectors can down-regulate each other [10, 11]. The production of IgE is enhanced by cytokines, such as IL-4, IL-5, IL-6, and tumor necrosis factor-α, and inhibited by IFN-γ, IFN-α, and transforming growth factor-β [12–15]. In addition, production of IgE is critically dependent on the Th1/Th2 bias after exposure to allergen [15–17]. Several animal models have been utilized to test various methods for suppressing IgE production, including antibodies to IL-4 and IFN-γ [18, 19]. Also, many approaches have been examined to prevent or inhibit IgE responses in experimental models of allergy [20, 21]. Moreover, it is expected that inducing a Th1 bias or reducing the Th2 response will prevent AR.

Vector development has been considered to be a key to the success of molecular therapy for intractable human diseases. Vectors with high efficiency and minimum invasiveness are needed. For this purpose, we have tried to convert viruses to non-viral vectors and finally developed the hemagglutinating virus of Japan (also known as the Sendai virus) envelope vector (HVJ-E; approximately 300 nm in diameter) [22]. HVJ-E can fuse with cell membranes [23], a process that requires two distinct glycoproteins on the viral envelope. We have previously shown that HVJ-E inactivated by UV irradiation or treatment with β-propiolactone lacks the ability to replicate and can be loaded with and used to deliver plasmid DNA or therapeutic molecules in vitro and in vivo [22, 24].

In the present study, we employed HVJ-E to develop an efficient needleless system for intranasal delivery of proteins. We demonstrated ovalbumin (OVA)-induced IFN-γ release from splenocytes after nasal immunization of healthy BALB/c mice with HVJ-E containing OVA (HVJ-E/OVA). Moreover, intranasal administration of HVJ-E/OVA to OVA-sensitive AR model mice reduced OVA-induced Th2 cytokine production and prevented the increase in plasma levels of OVA-specific IgE.

Materials and methods

Animals

Male BALB/c mice were purchased from Charles River Breeding Laboratories (Yokohama, Japan). The mice were 5 or 6 weeks old when used for the experiments. They were maintained in a temperature-controlled, pathogen-free room. All animals were handled according to approved protocols and the guidelines of the Animal Committee of Osaka University.

Preparation and administration of HVJ-E/OVA or HVJ-E/BSA–Alexa Fluor®488

The HVJ-E vectors were constructed by incorporating OVA (grade VII; Sigma, St. Louis, MO) or bovine serum albumin (BSA)–Alexa Fluor®488 conjugate (Alexa488–BSA; Molecular Probe, Eugene, OR) into inactivated HVJ particles (Z strain; Genome One Neo®; ISK Biosciences, Tokyo, Japan). Briefly, 1,000 hemagglutinating units (HAU; 1 HAU contains approximately 3×10^6 particles) of HVJ-E were mixed with 100 μg of OVA (10 μg/μl in phosphate-buffered saline [PBS]) or Alexa488–BSA (10 μg/μl in PBS) and 1.2 μl of 1% nonidet P40. After centrifugation, the viral particles were washed with 1-ml PBS to remove the detergent and unincorporated OVA or Alexa488–BSA. Following centrifugation, HVJ-E (1,000 HAU of HVJ-E/OVA and 3,000 HAU of HVJ-E/Alexa488–BSA) was suspended in 10 μl of PBS. The vector was stored at 4°C until use. The mice were treated by placing a 10-μl drop of PBS containing HVJ-E onto their nasal cavities using a micropipette, after which, the mice inhaled the suspension.

Alexa488–BSA and OVA incorporated into HVJ-E were detected by Western blotting using anti-BSA (B2901, Sigma) and anti-OVA (A6075, Sigma) antibodies, respec-

tively. Comparing the signal of each protein in HVJ-E with that before incorporation, we estimated incorporation efficiency of each protein into HVJ-E. Incorporation efficiency of Alexa488–BSA and OVA into HVJ-E was approximately 2.7 and 9.1%, respectively (data not shown). Consequently, 8.1 μg of Alexa488–BSA and 9.1 μg of OVA were delivered to the nasal cavities when the mice were treated with 3,000 HAU of HVJ-E/Alexa488–BSA and 1,000 HAU of HVJ-E/OVA, respectively.

In the intranasal treatment of healthy mice or AR model mice, 10 μl of HVJ-E/OVA, 10 μl of empty HVJ-E (total amount is 1,000 HAU) alone, 10 μl of OVA, 10 μl of a mixture of HVJ-E and OVA (MIX), and 10 μl of PBS (negative control) were administrated. In each case, 1,000 HAU of HVJ-E and 9.1 μg OVA were used.

Histological examination

Twenty-four hours after nasal challenge, the mice were anesthetized deeply and perfused from the left ventricle to the right atrium with 4% paraformaldehyde (PFA). Next, their heads were removed, fixed overnight with 4% PFA, and decalcified with 10% Na_4EDTA (EDTA, ethylenediaminetetraacetic acid) for 14 days. The nasal tissues were then cut into 10-μm coronal sections, stained with 4′,6-diamidino-2-phenylindole (DAPI), and observed under a fluorescence microscope.

AR model mice

BALB/c mice were immunized intraperitoneally with one injection per week for 3 weeks (weeks 0, 1, and 2) by injection with a mixture of 100 μl of OVA (1 μg/μl in PBS) and 100 μl of $Al(OH)_3$ (20 mg/ml, pH 7.5; Wako Pure Chemical Industries, Osaka, Japan) as an adjuvant, and 100 μg of OVA was administrated intranasally on week 2 based on the previous reports [25, 26].

Timeline of experiments using AR model mice

The experimental timeline is shown in Fig. 1. First, AR model mice were constructed. BALB/c mice were sensitized three times by intraperitoneal injection of OVA and alum and once by intranasal administration of OVA. Three weeks after the last sensitization, AR model mice were administrated with molecules (HVJ-E/OVA, HVJ-E, OVA, MIX, and PBS) once a week for 3 weeks. One week after the last therapeutic procedure, cytokines released from splenocytes were quantified by using enzyme-linked immunosorbent assay (ELISA). After the therapies, the mice were exposed to OVA. From 5 to 11 weeks after the first sensitization, blood was taken from the tail vein, and serum OVA-specific IgE was quantified by using ELISA.

Preparation of splenocytes

The mice were euthanized, and spleens were taken. The spleens were homogenized by using ground glasses in a Roswell Park Memorial Institute (RPMI) 1640 medium supplemented with 10% fetal bovine serum, 100 μg/ml streptomycin, and 100 U/ml penicillin. Splenocytes were homolyzed with the mixture of 4.5 ml of 0.83% NH_4Cl and 0.5 ml of 170 mM Tris–HCl (pH 7.65) for 5 min and washed twice with 10 ml of the medium.

Measurement of cytokine production by splenocytes

Murine splenocytes were seeded in 24-well plates (5.0×10^6 cells/well) in 1 ml of RPMI 1640 medium supplemented with 10% fetal bovine serum, 100 μg/ml streptomycin, and 100 U/ml penicillin. After a 96-h incubation in the presence or absence of OVA (50 μg/well) at 37°C in an atmosphere containing 5% CO_2, culture supernatants were harvested for measurement of IL-4, IL-5, and IFN-γ levels using ELISA kits (R&D Systems, Minneapolis, MN) according to the manufacturer's instructions.

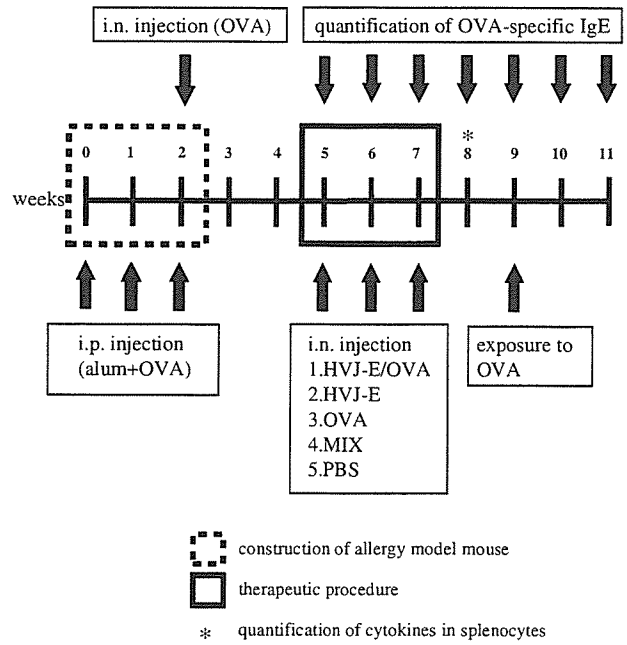

Fig. 1 Experimental timeline. Mice received intraperitoneal injection of OVA and alum for 3 weeks. Immediately after the last intraperitoneal injection, we administered OVA to the nasal cavities to induce AR. After 3 weeks, the mice were treated intranasally once per week for 3 weeks with HVJ-E/OVA, empty HVJ-E alone, OVA alone, MIX or PBS. Finally, the mice were exposed to allergen (OVA)

Quantification of OVA-specific serum IgE

Serum levels of OVA-specific IgE were quantified using a two-step sandwich ELISA. Plates (flat-bottomed 96-well; Becton Dickinson Labware, Franklin Lakes, NJ) were coated with purified anti-mouse IgE monoclonal antibody (2 μg/ml in PBS; PharMingen, San Diego, CA) at 37°C for 1 h. Subsequently, the plates were washed, blocked for 30 min at room temperature with 200 μl of 1% BSA in PBS, and washed three times with a washing buffer (0.05% Tween 20 in PBS). Serum samples were diluted in 1% BSA in PBS, added to the plates, and incubated for 1 h at room temperature. After washing three times with the washing buffer, the plates were incubated for 1 h at room temperature with OVA (10 μg/ml in 1% BSA in PBS). A detecting antibody (horseradish peroxidase-conjugated IgG

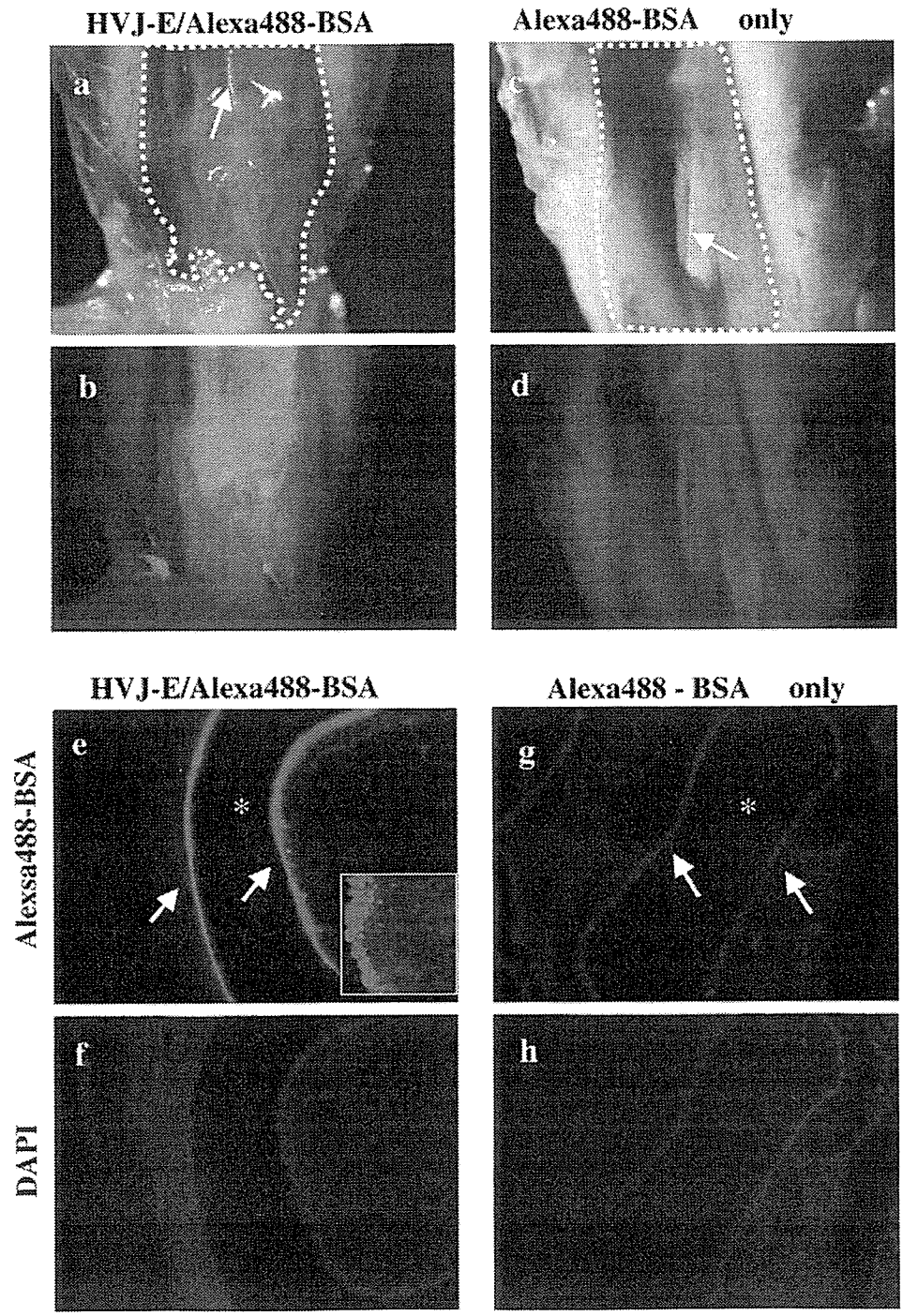

Fig. 2 Protein delivery to murine nasal mucosa using the HVJ-E system. Alexa488–BSA (*green*) was delivered to the murine nasal mucosa using HVJ-E (**a**, **b**, **e** and **f**) or without vector (**c**, **d**, **g** and **h**). (**b**) and (**d**) are fluorescence microscopic view of (**a**) and (**d**), respectively. *Arrows* in (**a**) and (**c**) indicate nasal septum; *arrows* in (**e**) and (**g**), nasal mucosa; *asterisks* in (**e**) and (**g**), nasal cavity. In (**f**) and (**h**), nuclei were stained with DAPI (*blue*). The *inset* in (**e**) shows a higher magnification merged view of the nasal epithelium after treatment with HVJ-E containing Alexa488–BSA. Original magnification, ×40 (**a**–**d**), ×400 (**e**–**h**), or ×1,000 (*inset* in **e**)

fraction of anti-OVA; Rockland, Gilbertsville, PA) was then added at a final dilution of 1:15,000. After incubating the plates for 30 min at room temperature, they were washed five times with the washing buffer. Finally, the plates were incubated for 15 min at room temperature with a substrate solution (ELISA POD Substrate TMB Kit Hyper; Nakalai Tesque, Kyoto, Japan) to allow color development. The reaction was terminated with a stop solution, and the absorbance at 450 nm in each well was measured with an ELISA plate reader (multi-plate reader Mithras LB940; Berthold Technologies, Wildbad, Germany). IgE levels were calculated as the fold increase over the plasma IgE level in the negative control mice.

Statistics

All results are expressed as means±standard error of mean. Data were compared using an unpaired Student's *t*-test for comparisons between the two groups and by analysis of variance followed by Dunnet's test for multiple comparisons. Differences were considered statistically significant when the *p* values were less than 0.05.

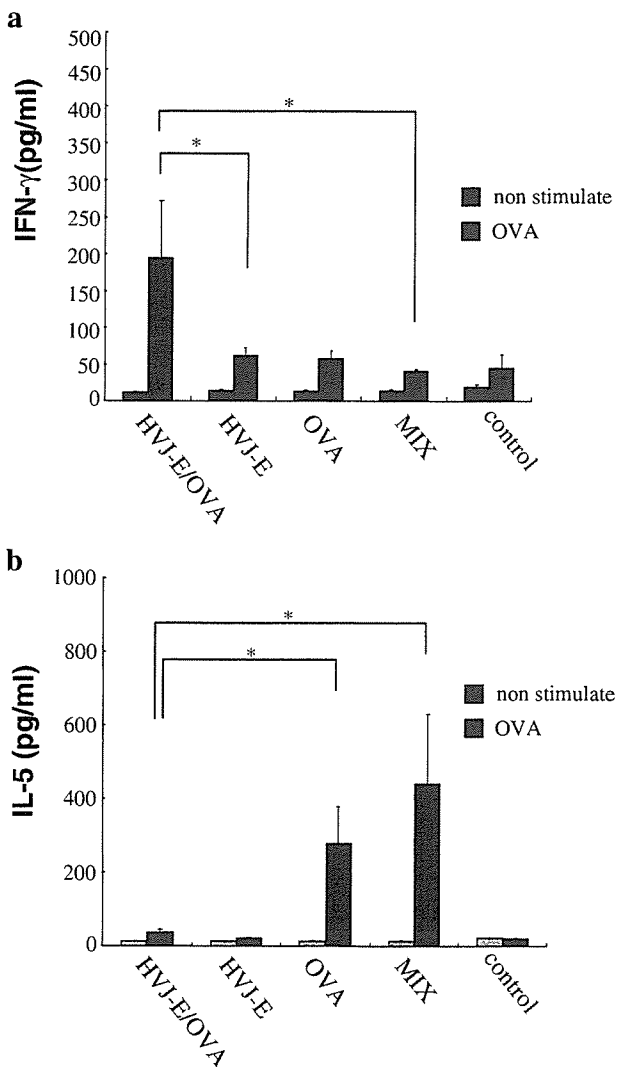

Fig. 3 Changes in the Th1/Th2 balance after intranasal sensitization in healthy mice. Expression of Th1/Th2 cytokines were examined in the mice (n=5 animals per group) receiving intranasal administration of HVJ-E/OVA, empty HVJ-E alone, OVA alone, MIX or PBS (negative control; n=5 animals per group) three times per week for 3 weeks. Splenocytes were isolated from the mice and incubated with or without OVA, after which, cytokine production was measured by ELISA. The HVJ-E/OVA group produced a higher level of IFN-γ (**a**) and lower level of IL-5 (**b**; *p<0.05). The OVA and MIX groups produced higher level of IL-5 (**b**; *p<0.05). The results are representative of three independent experiments

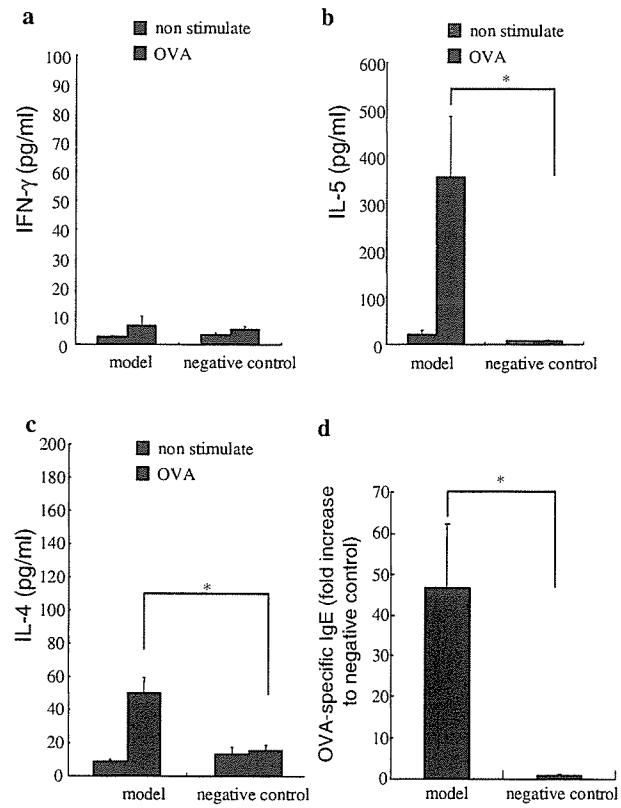

Fig. 4 Cytokines and IgE in AR model mice. Production of cytokines and IgE by splenocytes from AR model mice (n=5 animals per group). Compared to splenocytes from negative control mice, splenocytes from AR model mice produced higher levels of Th2 cytokines IL-4 (*p<0.01) and IL-5 (*p<0.05) and lower levels of the Th1 cytokine IFN-γ (**a**, **b** and **c**). AR model mice also produced exhibited serum levels of OVA-specific IgE (**d**; *p<0.05). The results are representative of three independent experiments